

## Numerical simulation of cooling effect of vegetation enhancement in a subtropical urban park



An-Shik Yang<sup>a</sup>, Yu-Hsuan Juan<sup>a</sup>, Chih-Yung Wen<sup>b,\*</sup>, Chao-Jui Chang<sup>a</sup>

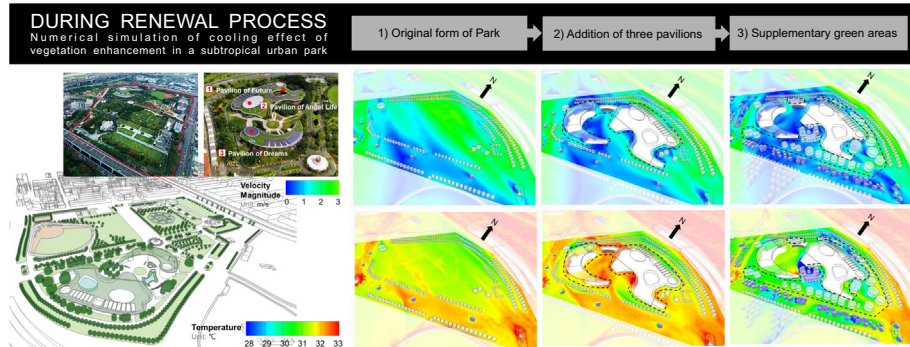
<sup>a</sup>Department of Energy and Refrigerating Air-Conditioning Engineering, National Taipei University of Technology, Taipei 106, Taiwan

<sup>b</sup>Department of Mechanical Engineering, The Hong Kong Polytechnic University, Kowloon, Hong Kong

### HIGHLIGHTS

- The cooling efficacy from vegetation implanted in a urban public park is studied.
- Three cases showing various types of greening in the park renewal were conducted.
- On-site measurements were also conducted to validate the CFD simulation results.
- The increase of GCR are linear with PET comfort area percentage.
- Results can be used as a guideline for the green sustainability.

### GRAPHICAL ABSTRACT



### ARTICLE INFO

#### Article history:

Received 5 September 2016

Received in revised form 16 January 2017

Accepted 27 January 2017

Available online 16 February 2017

#### Keywords:

Urban greening

Green coverage ratio

Physiological equivalent temperature

Urban heat island

CFD simulation

### ABSTRACT

Vegetation covers in urban parks are very useful for providing a cool microclimate which mitigates urban heat islands (UHIs). The objectives of this investigation are to therefore conduct on-site measurements and computational fluid dynamic simulations to evaluate the cooling efficacy from vegetation planted in a public park in Taipei, which is a subtropical city in Taiwan. The thermo-flow characteristics are predicted and compared with the measured air velocity and temperature data by using ultrasonic anemometers and an infrared camera to validate the computer modeling, including the sophisticated configurations of trees. Computations are also conducted to resolve the physiological equivalent temperature (PET) profiles for assessing the thermal comfort state at the pedestrian level of the outdoor environment. To investigate the impacts of park renewal on the urban microclimate, three pavilions and supplementary green areas are added to the simulation, and the results reveal that there is a better cooling effect in the park with a higher green coverage ratio (GCR). Moreover, the simulations find that the increased tree coverage ratio can more than compensate for loss of coverage of grasses, resulting in an overall decrease in average temperature. The relationship between thermal comfortable area and green coverage ratio tends to be nonlinear in nature. However, it would be more convenient for applications to adopt the linear regression analysis for determining the correlation between the GCR and PET for the percentage of areas that are comfortable ( $C_f$ ). It shows that  $C_f = 0.96 \times \text{GCR} + 5.08$ , with a reasonable  $R^2$  value of 0.91, for GCR ranged from 54.5 to 71.6%, indicating that there is a significant reduced UHI effect with increases in the GCR. In addition, the correlation implies that a completely thermally comfortable condition will prevail in the park if it has full green coverage. This correlation thus serves as an important guideline for urban planners and managers when designing and managing public urban spaces, such as parks.

© 2017 Elsevier Ltd. All rights reserved.

\* Corresponding author at: Department of Mechanical Engineering, The Hong Kong Polytechnic University, Hung Hom, Kowloon, Hong Kong.

E-mail address: [cyywen@polyu.edu.hk](mailto:cyywen@polyu.edu.hk) (C.-Y. Wen).

## Nomenclature

$C_f$	areas that are thermally comfortable with PET of 21.3–28.5 °C/the entire park area, in %	$T_a$	temperature of air
$C_d$	drag coefficient of plant elements	$T_f$	foliage temperature
$C_\mu$	turbulent constant, 0.09	$T_{ref}$	reference temperature
$C_{e1}$	turbulent constant, 1.44	$u^*$	friction velocity
$C_{e2}$	turbulent constant, 1.92	$u_{ABL}^*$	ABL friction velocity
$D$	leaf diameter	$u^+$	dimensionless mean streamwise wind speed
$E_0$	empirical constant, 30.0	$u_i$	velocity component in $i$ axis
GCR	areas covered by greenery/the entire park area, in %	$u_j$	velocity component in $j$ axis
$g_i$	gravity in $i$ axis	$U_{(z)ABL}$	mean inlet velocity of atmospheric boundary layer
$h$	sensible enthalpy	$x, y, z$	coordinates
$hc$	heat transfer coefficient	$x_i$	coordinates in $i$ direction
$I$	average turbulence intensity	$x_j$	coordinates in $j$ direction
$J_{f,h}$	direct heat flux	$z_0$	roughness length
$K$	von Karman's constant, 0.42	$\beta$	thermal expansion coefficient
$k$	turbulent kinetic energy	$\varepsilon$	turbulent energy dissipation rate
$L$	turbulence length scale	$\varepsilon_{ext}$	air emissivity of external field, 0.05
LAD	leaf area density	$\mu$	dynamic viscosity
$P$	turbulent production term	$\mu_t$	turbulent viscosity
$p$	pressure	$\mu_{eff}$	effective viscosity
$r_a$	aerodynamic resistance	$\rho$	density
$S_h$	energy source term that relates heat exchange at plant surface to atmosphere	$\rho_{ref}$	reference density
$S_k$	generation of turbulence	$\lambda$	molecular conductivity
$S_{u_i}$	source term of loss of wind speed owing to drag forces on plants	$\lambda_t$	turbulent conductivity
$S_\varepsilon$	dissipation of turbulence	$\tau_{ij}$	deviatoric stress tensor
$T$	temperature	$\sigma_k$	turbulent constant, 1.0
		$\sigma_e$	turbulent constant, 1.3

## 1. Introduction

Climate change is one of the most challenging issues to the environment, both today and in the near future. As urban development continues to increase, natural vegetation covers are being replaced with constructed buildings and urban infrastructures, thus resulting in the well-known urban heat island (UHI) effect which can noticeably increase the temperature in densely built-up urban areas during the summer months [1,2]. UHI represents a city or metropolitan area that is significantly hotter than its surrounding rural areas. Consequently, many studies have been conducted on the utilization of green space in moderating urban climates [3–11]. Urban parks are known to be essential for providing a cool microclimate and mitigating the UHI effect due to the vegetation cover [12–14]. Researchers have therefore consistently provided related ways to alleviate the UHI effect, such as increasing tree covered areas and density [14,15]. As well, green roofs and green walls on buildings are generally recognized as part of a sustainable building process that also mitigates the UHI effect [6,16–19]. In essence, trees and vegetation provide shading to buildings from solar radiation, and accordingly reduce the surrounding surface temperature. The ambient temperature can also be reduced through the evaporation and transpiration from vegetation. In addition, one or more rows of trees or shrubs planted could lower the wind speed and provide sheltered areas as a shelterbelt, and hence reduce wind-induced air infiltration in buildings [20,21]. At the same time, the shielding of wind by trees also contributes to maintaining a comfortable temperature inside buildings by reducing the amount of hot blowing wind in the summer [22]. Wang et al. [14] indicated that the cooling effect from tree shade tends to be more effective than that from the evapotranspiration of lawns, thus resulting in a considerable amount of energy saving and minimizing the cooling load. Simmons et al. [23] indicated the

great potential of implementing green roofs in subtropical regions with high temperatures and strong rain.

As climate change continues to intensify the severity of UHIs, the outdoor meteorological state has profound effects on the comfort sensation. Since high temperatures often exceed the human comfort threshold, a better understanding of perceived thermal conditions is important to improve the thermal comfort of the external environment for use and enjoyment. Based on a body heat-balance model, the physiological equivalent temperature (PET) has been applied in many outdoor thermal comfort standards as a common and useful bioclimatic index [24,25]. PET uses a universally known unit (°C) as a thermal indicator of the microclimate, and the results are easily understandable enough for possible users (including planners, decision-makers, and even the public) who are not familiar with modern human-bio meteorological terms [17,25,26]. The Munich energy balance model for individuals (MEMI), as the basis for the calculation of PET, is such a thermophysiological heat balance model. It is a universally applicable model to take all basic thermoregulatory processes into account, enabling the user to predict “real values” of thermal quantities of the body, i.e. skin temperature, core temperature, sweat rate or skin wetness [27,28]. The MEMI model is based on the energy balance equation for the human body:  $M + W + R + C + E_D + E_{Re} + E_{SW} + S = 0$ , where  $M$  is the metabolic rate,  $W$  is the physical work output,  $R$  is the net radiation of the body,  $C$  is the convective heat flow,  $E_D$  is the imperceptible perspiration,  $E_{Re}$  is the sum of heat flows to heat and humidity the inhaled air,  $E_{SW}$  is the heat flow related to the evaporation of sweat and  $S$  is the storage heat flow for heating or cooling the body mass; the unit of all heat flows is in Watt. The individual terms in this equation have positive signs if they result in an energy gain for the body and negative signs in the case of an energy loss ( $M$  is always positive;  $W$ ,  $E_D$  and  $E_{SW}$  are always negative). The individual heat flows are controlled by

the following meteorological parameters, including air temperature ( $C, E_{Re}$ ), wind velocity ( $C, E_{SW}$ ), air humidity ( $E_D, E_{Re}, E_{SW}$ ) and mean radiant temperature ( $R$ ). In addition, thermo-physiological parameters are required by heat resistance of clothing (clo) and activity of humans (in Watt). These temperatures are influenced by the integrated effect of all climatic parameters, which are in some kind of interrelation affecting each other. These interactions are quantifiable in a realistic way by means of heat balance models. PET is defined to be equivalent to the air temperature that is needed to reproduce in a standardised indoor setting and for a standardised person. The core and skin temperatures are observed under the conditions being assessed [27,28]. Therefore, good design practices and policy implementation that improve the thermal comfort in city public parks are important for the enjoyment of public spaces.

The methods used to investigate the effectiveness of vegetation in enhancing cooling and mitigating the UHI effect are generally carried out through remote sensing [29–31], field measurements at the ground level [32–34], controlled experiments [35], and computational fluid dynamics (CFD) [11,36–47]. However, CFD are a cost-effective and practical way to reasonably predict the characteristics of outdoor urban microclimates in detail so as to appraise the effectiveness of vegetation covers. Several vegetation models have been proposed and assessed in the literature that reproduce the aerodynamic effects of trees on the airflow [38,43–45]. In addition, Taha developed a vegetation model that uses trees, green roofs and high albedo surfaces as strategies to mitigate the UHI effect [40]. Bruse and Fleer [36] utilized a CFD model that simulates the microclimate, ENVI-met, to study the impacts of ground green coverage on heat stress over a small park. Dimoudi and Nikolopoulou [11] used CFD modeling to examine the cooling effects of different vegetation arrangements in a generic building setup. Alexandri and Jones [39] conducted a study which used CFD modeling to explain for the thermal influences of green walls and roofs on the microclimate for nine different climates and urban canyon geometries. Vidrih and Medved [42] validated a three-dimensional (3D) CFD model by comparing the measured results with predicted air temperatures from tree crowns, thus demonstrating the effectiveness of CFD modeling to accurately simulate the thermo-flow processes in a city park environment. Srivanit and Hokao [37] focused on the strategies of greening modification by adding more greening areas with on-site measurements and a CFD simulation model that uses ENVI-met.

Although there are a number of modeling studies on the vegetation cooling effects and the development of UHI effects on the microclimate in urban regions, the majority of the computational models mainly consider relatively simplified geometries of the target areas which comprise trees, buildings, and streets (i.e. the object site and relative contiguous surroundings) treated. Relatively few efforts have been attempted to model realistic urban environments with detailed geometries of the buildings and street canyons and study the associated interactions of vegetation cover with the airflow and thermal behavior in hot and humid regions. Moreover, many research works have been conducted in the USA [48], Greece [49], Portugal [13], Dubai [10] and Japan [9,37,50,51] on the UHI effect in urban planning. There are very few studies related to the subtropical areas [52], particularly in the use of field measurements and CFD simulations for quantitative evaluation. Therefore, the goal of this research is to perform on-site measurements and CFD simulations to assess the vegetation efficiency of a public park (with different types of greening, e.g. trees and plants, green roofs and grass lawns) and its influence on the atmosphere of a bordering locality in a densely urbanized area in a subtropical region, which has a hot and humid climate.

To validate the simulated modeling, the predicted steady velocities and directions of the wind are compared with the measure-

ment data acquired by ultrasonic anemometers. In addition, the temperature distributions are computed and compared with the images visualized by using thermography which are taken with an infrared camera. The computed velocity and temperature fields are then utilized to determine the PET values for appraising the thermal comfort state at the pedestrian level of the outdoor environment. Numerical simulations are used to investigate the effects of adding three pavilions and supplementary green areas on the urban microclimate in the park renewal process. The effectiveness of vegetative amenities on reducing the PET in urban public spaces will be examined. The findings of this research will support better prediction of the effects of park renewal and serve to improve thermal comfort by optimizing the GCR in a subtropical region, thus helping urban planners and managers mitigate increases in temperatures to enhance building energy efficiency associated with climate change as well as to enable the effective thermal adaptation of urban public spaces, and promote environmental sustainability.

## 2. Methodology

### 2.1. Study site

The study site in this research work is called Xinsheng Park, which was part of an urban redevelopment project in Taipei, Taiwan. The Taipei city government unveiled three new pavilions ("Pavilion of the Future", "Pavilion of Angel Life" and "Pavilion of Dreams") in the park for the 2010 Taipei International Flora Exposition. The pavilions were designed by a local architect, Chang Ching-Hwa, and constructed around old trees with their rooftops and walls populated by vegetation. After the expo, all of the pavilions were to serve as activity venues for public events. During the park renewal, considerable endeavors were made to preserve the original conditions of the park with improvements primarily in the form of adding more green areas. The key reason for the design to incorporate vegetation with different greening types was to create a positive impact on the comfort level of users by reducing the air temperature.

**Fig. 1** illustrates: (a) the location of the study site, Xinsheng Park, on a Google map and shows (b) pictures of Xinsheng Park, and (c) three new pavilions (Pavilion of the Future, Pavilion of Life and Pavilion of Dreams) after the renewal process. The study site is located in northern Taiwan (25°04'16.1"N and 121°31'53.0"E) and the second largest urban public park in Taipei, which covers an area of 19.5 ha. Taipei has a humid and subtropical climate. The meteorological data (over the past thirty years) of Taipei, which are the monthly mean, maximum and minimum air temperatures are provided in **Fig. 2**. As shown in the figure, the coolest and warmest months are January and July, with mean temperatures of 16.1 °C and 30.4 °C, respectively. In addition, a previous study by Lin et al. found that the maximum intensity of UHI occurs at noon in the summertime in Taipei, with a heat island intensity of 4.9 K [53]. Therefore, this paper will focus on the summer microclimate of Xinsheng Park.

### 2.2. On-site measurements

Experiments were conducted to assess the outdoor environment to characterize the microclimate of Xinsheng Park. For the field measurements, we applied for permission to the Parks and Street Lights Office, Public Works Department, Taipei City, to access Xinsheng Park for 11 days in July 2014, when we subsequently made the measurements (see **Table 1**). The reason for choosing this time period is primarily because there is a stronger cooling effect in the park in the summer as opposed to the winter,

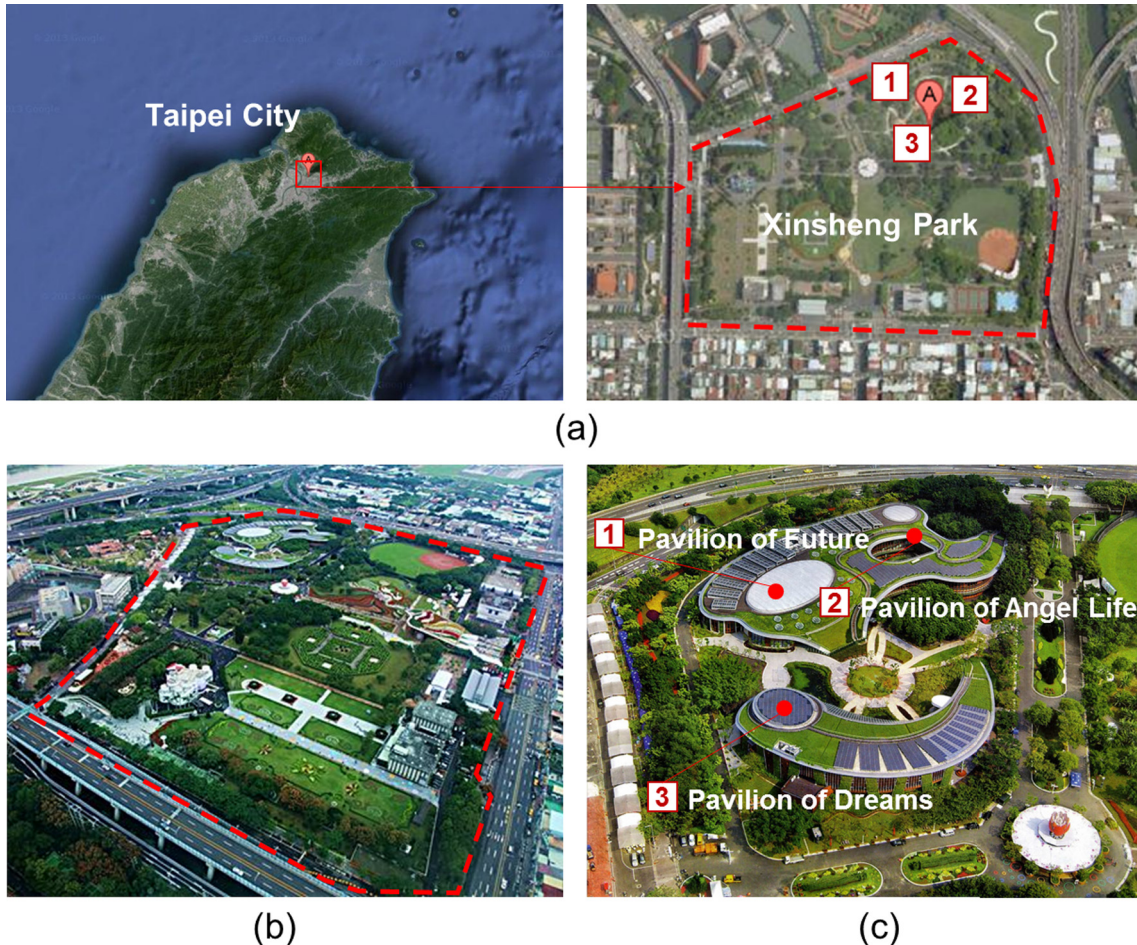


**Fig. 1.** (a) Xinsheng Park location: Google map (<http://maps.google.com>); pictures of (b) Xinsheng Park and (c) three new pavilions (Pavilion of the Future, Pavilion of Life and Pavilion of Dreams) after park renewal.

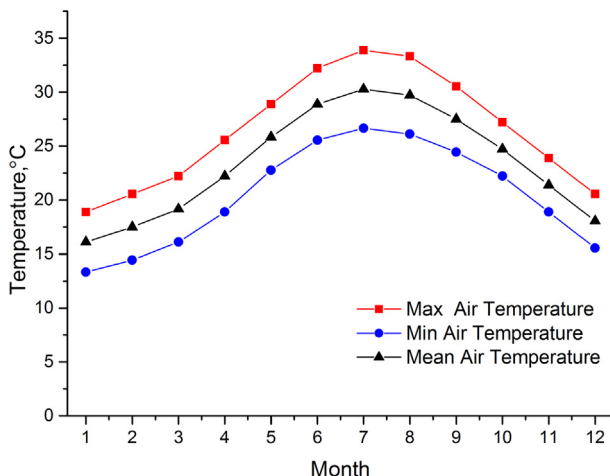


**Fig. 2.** Meteorological data (over past thirty years): monthly mean, maximum and minimum air temperatures in Taipei (Courtesy of the Central Weather Bureau).

and the cooling effect is also much stronger at noon compared to night time, according to the temperature measurement results from Chang et al. [54]. To highlight the cooling effect, we only focused on the data from three days (July 9, 13 and 17) when the sunshine rate was greater than 50% and ruled out rainy and cloudy days. The average reference velocities measured on July 9, 13 and

17 at Point R on the rooftop of the Pavilion of Dreams (height of 19 m above the ground) are 3.72 m/s, 2.93 m/s and 4.84 m/s, respectively, which are in good agreement with the meteorological data, as indicated in Table 1. Therefore, the data from July 9, 13 and 17 under clear-sky conditions were utilized to validate the CFD simulations.

The measurement instruments were selected in accordance with the specifications outlined in ISO 7726:1998 [55] (see Table A.1 in the Appendix). Fig. B.1 in the Appendix shows the photographs and locations of the 15 monitoring points in Xinsheng Park. The corresponding images of the monitored points are also shown. The velocities and directions of the wind were measured at a height of 1.75 m, except for the reference velocity measured at Point R. The measurements were carried out with four 3-axis ultrasonic anemometers (WindMaster, Gill Instruments Limited). The windspeed range is 0–45 m/s, and the resolutions are 0.01 m/s and 0.1°. Their accuracy is <1.5 RMS for wind incidences up to an angle of about 30° from the horizontal axis. Due to the limited number of anemometers, the experimental procedures of Blocken et al. [56] were adopted to measure the wind velocities and directions at the 15 monitored points. Two types of measurements were conducted: (1) measurements taken at one fixed position (Point R on the rooftop of the Pavilion of Dreams) for a period of 11 h (7:00 to 18:00 h, July 17, 2014) and (2) to cover all monitoring positions, measurements of 3 other mobile ultrasonic anemometers were taken in 14 different positions for a period of 50 min, see Fig. B.1 in the Appendix. The frequency of measure-

**Table 1**

Meteorological data for July 8–18, 2014 from local meteorological station. Also shown: average data for entire month of July (Courtesy of Central Weather Bureau (Taiwan)).

Data	Local meteorological station				
		Sunshine rate (%) <sup>*</sup>	Air temperature (°C)	Wind velocity (m/s)	Rainfall (mm)
8 July	Rainy	10.3	29.6	3.7	14 (from 7:48)
9 July	Sunny	57.5	32.9	3.7	
10 July	Cloudy	14.0	32.3	2.8	
11 July	Rainy	25.8	31.2	3.0	2.5 (from 18:57)
12 July	Cloudy	34.7	31.5	2.9	
13 July	Sunny	57.6	33.0	2.9	
14 July	Rainy	30.3	31.2	2.8	28.5 (from 15:59)
15 July	Rainy	40.7	31.0	3.9	29.5 (from 17:50)
16 July	Cloudy	48.2	31.4	4.2	
17 July	Sunny	66.7	30.4	4.8	
18 July	Cloudy	49.0	32.2	4.1	
July 2014 (on average)		65.9	30.5	4.8	

\* Sunshine Rate(%) = the ratio between sunshine duration and daylight duration of the day.

ment for all positions was at least 1 Hz. For data acquisition and analysis, the wind sensors were managed with a Windows®-based computer program to read, debug, record and control the data transferred from each ultrasonic anemometer.

Moreover, thermographic images which have a high image quality of 640(H) × 480(V) pixels were recorded by using an infrared camera (Thermal Imager Avio/NEC, H2640) with a noise equivalent temperature difference (NETD) sensitivity of 0.03 °C and accuracy of 2 °C. Measurements of the outdoor temperature and mean radiation temperature were taken separately by using a thermal flow probe (Testo 0635 1543) with a radiation shield and a globe probe (Testo 0602 0743, globe diameter of approximately 150 mm) with an accuracy of 0.5 °C (with a measuring range of −20 °C to 70 °C) at heights of 1.75 and 1.1 m, respectively, above the terrain. The thermal flow and the globe probes were traversed across all 15 monitoring sites, and the same experimental procedure for measurement of the wind speed and direction was repeated (for the period when the measured temperatures are steady).

### 2.3. Computational approach

A theoretical model formulated in the ANSYS/Fluent® software was utilized to simulate the terrestrial wind that flows over Xinsheng Park [57]. The park consists of three pavilions in which the Pavilion of Dreams is 120 m × 60 m × 19 m, whereas the Pavilions of Angel Life and the Future are connected together with combined geometric dimensions of 200 m × 140 m × 14 m. The forms of the building models and the topography of the object site were specifically recreated by obtaining their extents and curving details from 3D shape drawings provided by the architect. The preprocessor of the CFD software ANSYS Fluent® ver. 14 could easily incorporate the solid model to generate a numerical model by the grid generator module, ANSYS Meshing® [57]. Numerical computations were then conducted by ANSYS Fluent® software to resolve the air velocity and temperature fields to investigate the processes of the wind across the buildings and vegetation. The investigation was based on steady 3D conservation equations of mass, momentum and energy for the incompressible turbulent flow. The governing equations are given as below:

$$\frac{\partial u_i}{\partial x_i} = 0, \quad (1)$$

$$\frac{\partial \rho u_i u_j}{\partial x_j} = -\frac{\partial p}{\partial x_i} + \frac{\partial}{\partial x_j} \left[ (\mu + \mu_t) \left( \frac{\partial u_i}{\partial x_j} + \frac{\partial u_j}{\partial x_i} \right) \right] + \rho_{ref} g_i \beta (T - T_{ref}) + S_{u_i}. \quad (2)$$

where  $u_i$  represents the air velocity component in the  $i$  axis;  $p$ ,  $\rho$ ,  $T$ ,  $\mu$ ,  $\mu_t$ ,  $g_i$  and  $S_{u_i}$  signify the pressure, density, temperature, dynamic viscosity, turbulent viscosity, gravity acceleration and source term that describes the loss of wind speed owing to drag forces from plants, respectively. The model in this study treats density as a constant value in all of the equations, except for the buoyancy term in the momentum equation. The Boussinesq approximation,  $\rho = \rho_{ref} \beta (T - T_{ref})$  in Eq. (2), was employed to model the buoyancy-driven flow [3], where  $\beta$ ,  $T_{ref}$  and  $\rho_{ref}$  signify the thermal expansion coefficient, reference temperature and reference density. The properties of air at 30.4 °C (the mean radiation temperature of Xinsheng Park from 10:00 to 17:00 h, July 17, 2014) and 1 atmospheric pressure were used to the thermo-flow calculations. Besides, the energy equation is expressed by a sensible enthalpy  $h$  as:

$$\frac{\partial \rho u_i h}{\partial x_j} = \frac{\partial}{\partial x_j} \left[ (\lambda + \lambda_t) \left( \frac{\partial T}{\partial x_j} \right) \right] + \tau_{ij} \frac{\partial u_i}{\partial x_j} + S_h. \quad (3)$$

where the terms  $\lambda$  and  $\lambda_t$  are the molecular and turbulent conductivities, respectively,  $\tau_{ij}$  is the deviatoric stress tensor, and  $S_h$  the energy source term related to heat exchange at the plant surface to the atmosphere. A detailed description of  $S_h$  will be given later.

To select the turbulent model, the realizable  $k-\varepsilon$  model, developed by Shih et al. [58], has demonstrated substantial improvements over the standard  $k-\varepsilon$  model for simulations of flows that involve separation, vortices, rotation, and recirculation [59–61]. In this work, the intricate geometry of Xinsheng Park suggests a complex flow phenomenon, and thus the realized  $k-\varepsilon$  model was adopted for turbulence closure, as follows:

$$\frac{\partial \rho u_i k}{\partial x_i} = \mu_t S^2 - \rho \varepsilon + \frac{\partial}{\partial x_i} \left[ \left( \mu + \frac{\mu_t}{\sigma_k} \right) \frac{\partial k}{\partial x_i} \right] + S_k, \quad (4)$$

$$\frac{\partial \rho u_i \varepsilon}{\partial x_i} = C_1 S \rho \varepsilon - C_2 \frac{\rho \varepsilon^2}{k + \sqrt{v \varepsilon}} + \frac{\partial}{\partial x_i} \left[ \left( \mu + \frac{\mu_t}{\sigma_\varepsilon} \right) \frac{\partial \varepsilon}{\partial x_i} \right] + S_\varepsilon, \quad (5)$$

where  $\mu_t$  is  $\mu_t \rho k^2 / \varepsilon$ ,  $k$  the turbulent kinetic energy,  $\varepsilon$  the turbulent energy dissipation rate and variable  $S = (2S_{ij}S_{ij})^{0.5}$  with  $S_{ij} = 0.5(\partial u_i / \partial x_j + \partial u_j / \partial x_i)$ . The factor  $C_1 = \max [0.43, \eta / (\eta + 5)]$  and  $\eta = S(k/\varepsilon)$ . The constants  $C_2$ ,  $\sigma_k$  and  $\sigma_\varepsilon$  are 1.0, 1.0 and 1.2, respectively. The density, viscosity and conductivity of air are 1.163 kg/m<sup>3</sup>,  $1.877 \times 10^{-5}$  N s/m<sup>2</sup> and 0.0265 W/m k, respectively, at a mean temperature of 30.4 °C.

In the simulation, the vegetation cover was modeled as a porous medium to interact with the airflow. Specifically, the source terms were added to the transport equations in Eqs. (2)–(5) to account for the effects of vegetation on the airflow and temperature. In Eq. (2), the local source term  $S_{u_i}$  can be expressed as follows [62]:

$$S_{u_i} = -\frac{1}{2} \rho \cdot C_d \cdot LAD \cdot u_i \cdot u, \quad (6)$$

where  $C_d$  is the drag coefficient of the plant elements,  $u$  the velocity magnitude and  $LAD$  the leaf area density in  $\text{m}^2 \text{ m}^{-3}$  of the plant. A specified value of  $C_d = 0.2$  is used in this study, following many prior modeling studies [36,45,62–65]. The trees were treated as a one-dimensional (1D) column with a given normalized leaf area density (LAD) profile with height [36]. Different types of vegetation can be easily mimicked by using various non-uniform vertical distributions of LAD [66]. Srivani and Hokao [37] proposed a plant profile diagram approach from a typical image of a tree at the study site, thus producing a LAD profile parameterized for computations based on the observed LAD measurements. Essentially, LAD describes the distribution of the leaf area as a function of height, which prescribes the crown shape and height of the trees and hedges. As shown in Fig. B.2 in the Appendix, four types of trees are planted in different parts of the park: *Sterculia foetida*, *Dillenia indica*, *Ficus microcarpa* and *Ficus benjamina*. These trees have been successfully used as street trees in various urban tree systems in Taiwan. *Sterculia foetida* is a large, straight, deciduous tree that can grow to a height of 20 m or more. *Dillenia indica* is a medium size deciduous tree. *Ficus microcarpa* is a lush and very popular evergreen tree. *Ficus benjamina* is 30 m in height in natural conditions and commonly known as the weeping fig tree, and a very large and stately tree found in parks and other urban environments, such as wide roads. All four vegetation species were parameterized with the observed LAD profiles of the formed plants in terms of trees, tree height, and canopy width and height. The data were then written into user-defined functions (UDFs) to characterize the 3D canopy of the green features in the CFD simulations [57].

In the energy conservation equation (Eq. (3)), the source term  $S_h$  is used to relate heat exchange at the plant surface to the atmosphere and treat evaporation and transpiration from vegetation. Following the same procedure in Gromke et al. [63], a volumetric cooling power,  $S_h$  of  $250 \text{ W m}^{-3}$  for an LAD of unity ( $LAD = 1 \text{ m}^2 \text{ m}^{-3}$ ), was assigned to the numerical cells that contained vegetation and model the cooling effect of trees on the ambient air. In the simulations,  $S_h$  was set to  $250 \times \text{LAD}$  for the four types of trees and grass. The LAD of grass was set as  $4 \text{ m}^2 \text{ m}^{-3}$  with 0.2 m height.

Compared to an approach at the microscale level in which the latent heat fluxes from the leaves that pass through stomata pores are considered [67–69], this approach can be thought of as an integral and relatively coarse scale method. In Eqs. (4) and (5), the local source terms  $S_k$  and  $S_e$  model the generation and the dissipation of turbulence by the plants. They can be expressed by [62]:

$$S_k = \rho \cdot C_d \cdot LAD \cdot u_i^3 \quad (7)$$

$$S_e = \frac{\varepsilon}{k} \cdot \rho \cdot C_d \cdot LAD \cdot u_i^3 \quad (8)$$

Eqs. (6)–(8) were implemented as the UDFs in the CFD simulations to model the effects of vegetation on air flow and temperature [57].

The atmospheric boundary layer (ABL) flow was adopted to simulate the related atmospheric processes at the inflow boundary [70,71]. Fig. 3(a) illustrates the wind rose chart for Xinsheng Park at a height of 16 m in July 2014 from a local weather station. In view of the wind states in terms of the speed, direction and probability, the wind speed occurs most frequently at 4.85 m/s from the south east ( $113^\circ$ ) side of Xinsheng Park in July 2014, which was employed to determine the neutral ABL velocity,  $U_{ABL}$ , turbulent kinetic energy,  $k$ , and turbulence dissipation rate profiles,  $\varepsilon$ , as the incoming airflow conditions at the inlet [72,73].

$$U_{ABL} = \frac{u_{ABL}^*}{K} \ln \left( \frac{z + z_0}{z_0} \right) \quad (9)$$

$$k = \frac{(u_{ABL}^*)^2}{\sqrt{C_u}} \quad (10)$$

$$\varepsilon = \frac{(u_{ABL}^*)^3}{K(z + z_0)} \quad (11)$$

The ABL friction velocity  $u_{ABL}^*$  can be computed from a specified velocity  $U_h$  at a reference height  $h$  as below.

$$u_{ABL}^* = \frac{KU_h}{\ln \left( \frac{h+z_0}{z_0} \right)} \quad (12)$$

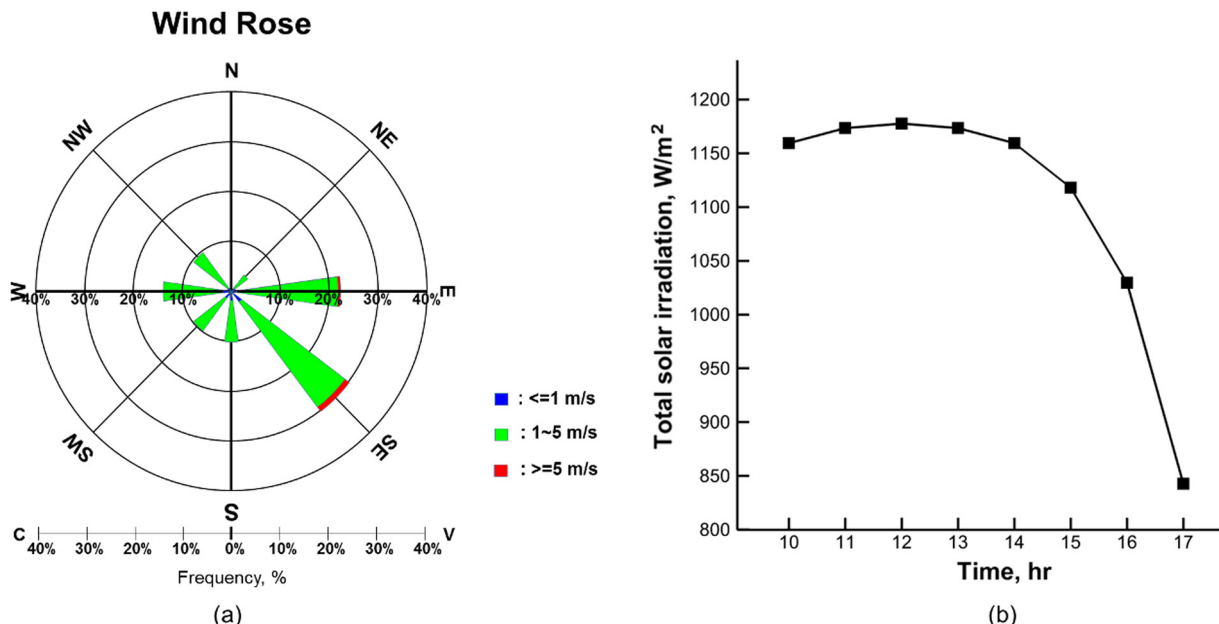
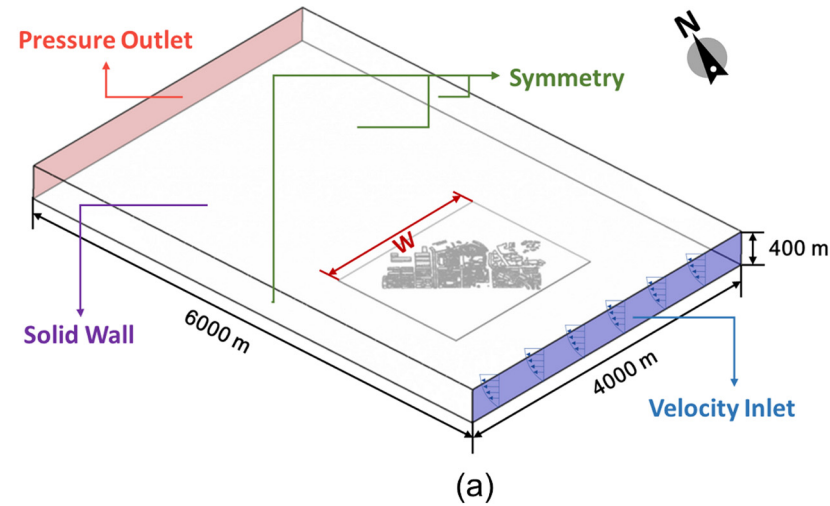


Fig. 3. (a) Wind rose chart for Xinsheng Park at height of 10 m in July 2014 and (b) variations of total solar irradiation from 10:00 to 17:00 h on July 17, 2014.

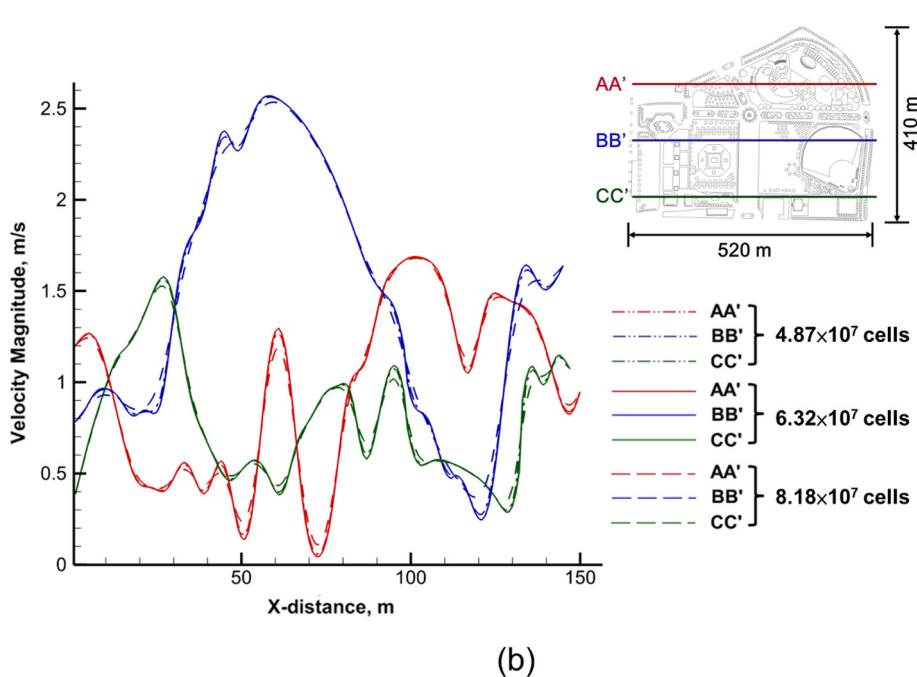
where  $K$  and  $z_0$  denote the von Karman's constant ( $\approx 0.4$ ) and the aerodynamic roughness. We used Eqs. (9)–(11) to acquire the mean inlet velocity at a height of  $z$  ( $U_{ABL}$ ),  $k$  and  $\varepsilon$  profiles in the ABL. In essence, the aerodynamic roughness can increase the drag when the wind crosses the terrain surface, indicating that the base of the standard wall function method by using the logarithmic law for the velocity profile is invalid in the presence of aerodynamic roughness [74,75]. In ANSYS Fluent®, the effect of real blockages to the wind was simulated by a wall roughness function to model the drag (from barriers) imposed on the ground surface. In consideration of the area that borders Xinsheng Park, the aerodynamic roughness was prescribed as 2 m ( $z_0$ ) based on the updated Davenport roughness classification for the city center with a complex that involves high-rises and low-rise concrete frame mixed-use commercial and residential buildings [76].

In this study, the radiative heat fluxes are required to be considered to accurately resolve the wall surface temperatures because of the significant radiation effect, as compared to the heat transfer

rates from convection or conduction. Hence, the solar radiation was computed by using the Solar Calculator dialog box in ANSYS Fluent®, which imposes incident radiation on the exposed surfaces in accordance with the position of the sun, which varies with time, date and global location [57]. Given that the latitude and longitude geographic coordinates of Xinsheng Park are  $25^{\circ}04'16.1''N$  and  $121^{\circ}31'53.0''E$ , respectively, Fig. 3(b) illustrates the variations in total solar irradiation on July 17, 2014. In addition, the solar load model in ANSYS Fluent® was used to determine the radiation load with discrete ordinates (DO). The solar irradiation was directly applied into the DO model to determine the radiant heat fluxes between the surfaces of the computational domain by solving the radiation intensity transport equations (RTEs) for gray diffuse walls. The structures in the park were made of concrete, whereas the streets were covered with asphalt in the calculations. Table A.2 in the Appendix presents the spectral optical properties and thermophysical properties of the involved materials [77]. The air emissivity of the external field  $\varepsilon_{ext}$  is 0.05 with an external radiation tem-



(a)



(b)

**Fig. 4.** (a) Computation domain with boundary conditions; (b) predicted velocity magnitude along three axial lines (at height of 1.75 m) of Xinsheng Park for three different grids.

perature of 36.5 °C. In addition, the heat transfer coefficients ( $h_c$ ) of the building surfaces were evaluated with the following empirical correlation, which is independent of the wind direction and suitable for high wind velocities [78,79]:

$$h_c = 5.7 + 3.8V_{air} \quad (13)$$

where  $V_{air}$  is the airflow velocity. In the simulations, the plants were modeled as a semi-transparent phase in the radiative modeling.

Some of the solar radiation incidents on the trees were reflected, whereas others tended to penetrate through the tree canopy due to the absorption and transmission of solar radiation [62].

Fig. 4(a) shows the computational domain with boundary conditions. To vary the boundary conditions at the outlet, a constant static pressure (1 atm) was employed at the exit of the calculation domain. The zero normal gradients of  $p$ ,  $k$  and  $\epsilon$  were imposed on the solid surface, with log-law wall functions applied for the next-

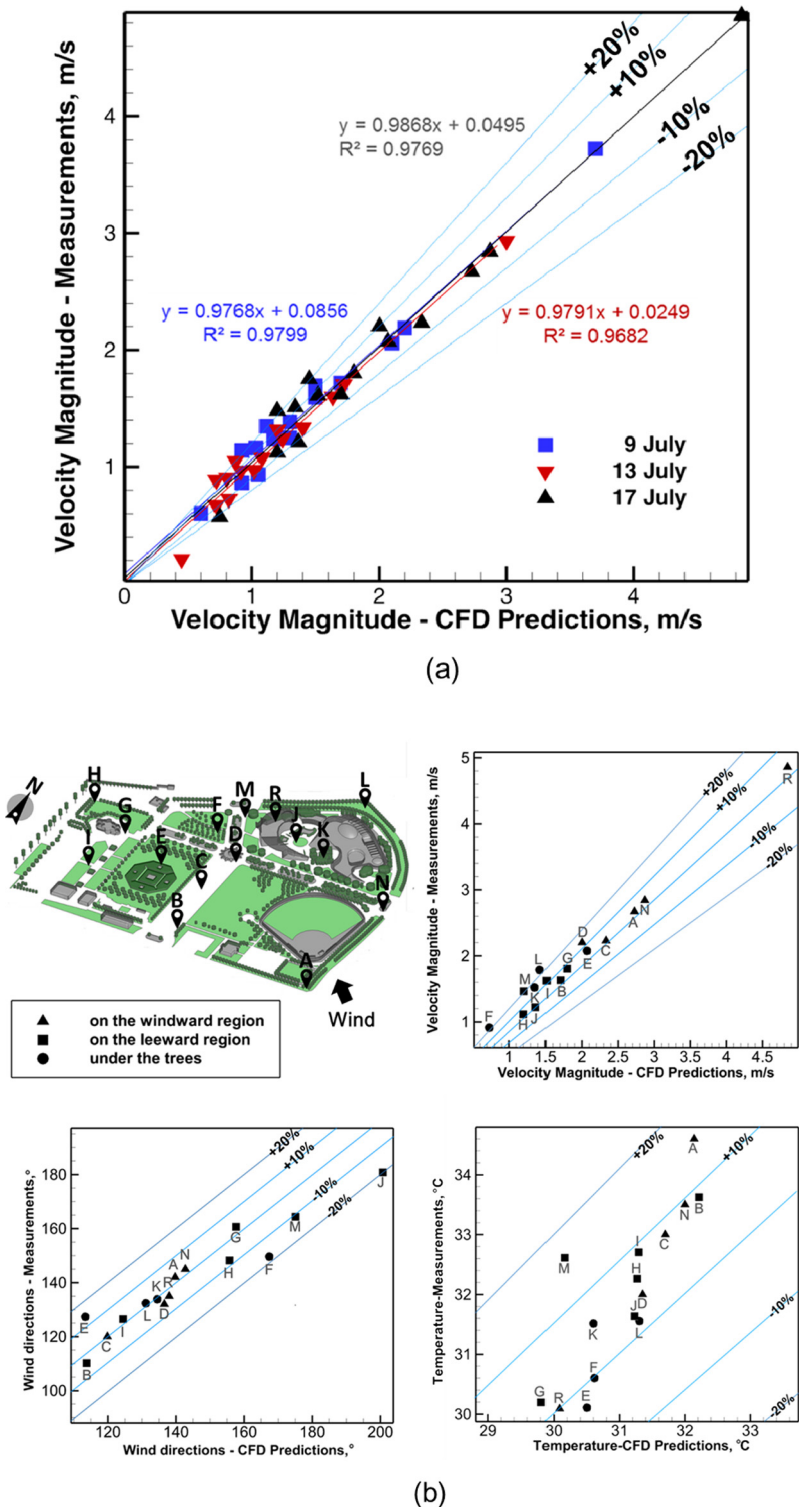


**Fig. 5.** Comparison of CFD predictions with measurements of (a) magnitude of air velocity on July 9, 13 and 17 and (b) magnitude of air velocity, wind direction and temperature at different monitoring locations on July 17.

to-surface grids of buildings [74]. The top and lateral boundaries were placed at a height of  $10 H$  from the ground and width of  $1.5 W$  from the centerline of the computational domain, where  $H$  and  $W$  are the maximum height of the object buildings and the width of the built area, respectively. Symmetry boundary conditions were employed by prescribing the zero normal component of velocity and zero normal derivatives for all flow variables at the top and lateral boundaries.

The aforesaid mathematical equations were discretized by using a finite control volume technique. In this study, a second-

order accurate central difference scheme is used to model the convective terms with adaptive damping to resolve non-physical oscillations. To appraise the diffusion terms, a second-order accurate central difference scheme was employed in the numerical solutions. An iterative semi-implicit method for pressure-linked equations consistent (SIMPLEC) numerical method was used for the coupling of velocity and pressure [80,81]. A steady solution was obtained with the convergence of the normalized residual errors of the flow variables ( $u$ ,  $v$ ,  $w$ ,  $p$ ,  $T$ ,  $k$  and  $\epsilon$ ) to  $10^{-5}$  and a mass balance check below 1% to achieve the wind field environments.

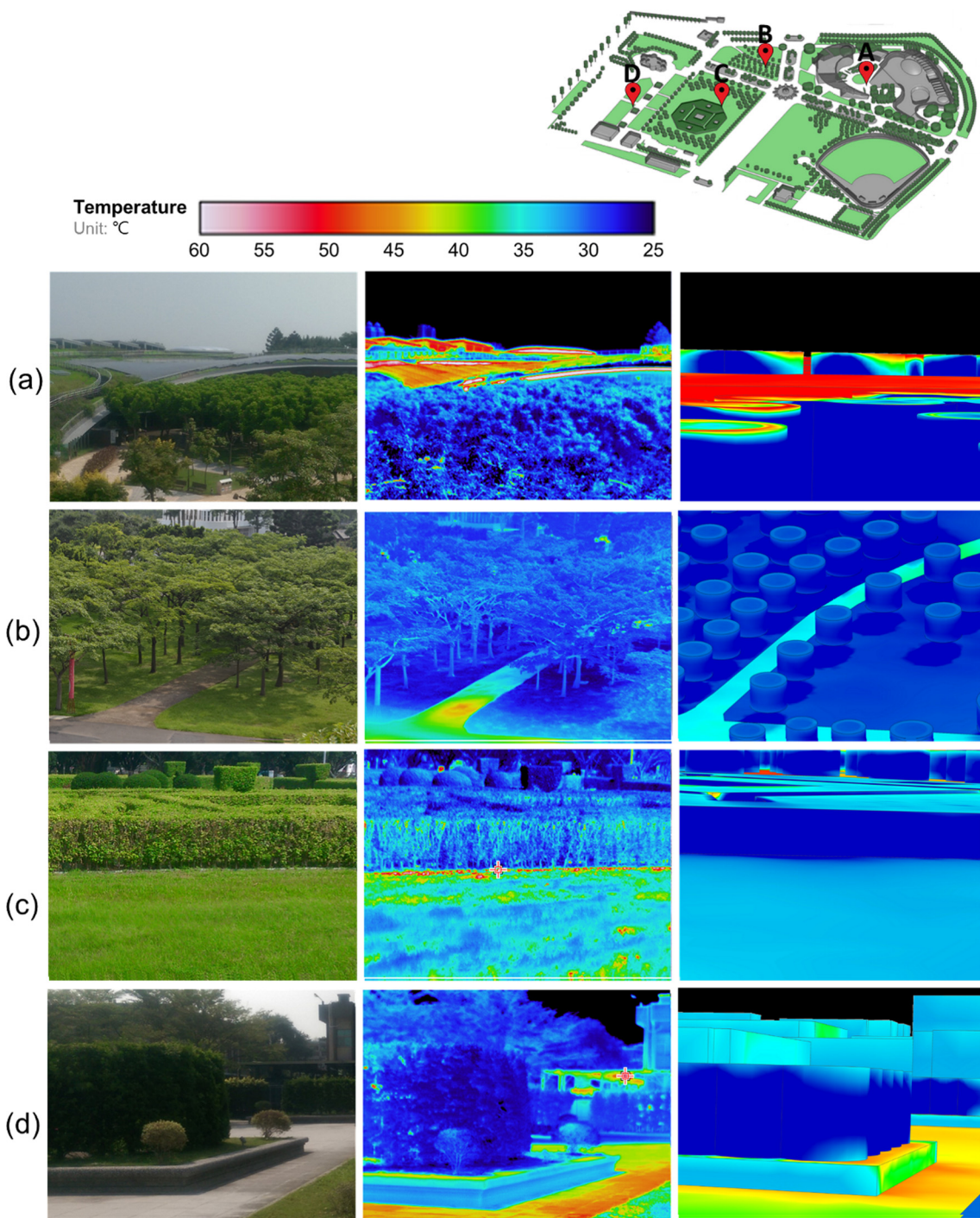


**Fig. 6.** Comparison of CFD predictions with surface temperature images visualized by using an infrared camera at different monitoring locations (with real scene photos).

### 3. Results and discussion

Simulation of realistic urban environments is carried out in this study with detailed geometries of buildings and street canyons to explore the effects of vegetation cover on the associated flow and thermal processes. The CFD simulations are conducted by using ANSYS/Fluent® and the resultant computational model is validated by comparing the predictions with the measurement results. Fig. 4(b) illustrates the magnitude of the predicted air velocity along three axial lines (at a height of 1.75 m) at Xinsheng Park for three different grids. The mesh system comprises two major sections: Xinsheng Park and the surrounding domain. Finer grids are placed in the areas that adjoined the trees and near the solid surface boundaries of the structures. The average cell length of the district around Xinsheng Park is around 0.63 m, with the smallest spacing of 0.019 m to resolve large variations of the flow properties related to the interaction of the wind with the structures. Calculations are carried out on the total number of grids of  $4.87 \times 10^7$ ,  $6.32 \times 10^7$ , and  $8.18 \times 10^7$ . The size of the computational domain is 6000 m in length, 4000 m in width and 400 m in height, respectively. The greatest difference between the computed magnitude of the air velocity and the measured data is 20.7% with a total number of grid points of  $4.87 \times 10^7$  and  $6.32 \times 10^7$  at a height of 1.75 m. However, the peak discrepancy of the predictions is reduced to 3.2% for the meshes of the grids of  $6.32 \times 10^7$  and  $8.18 \times 10^7$ . Since an increase in the total grids could increase the computational time, the above calculated results indicate that satisfactory grid independence may be achieved by using a mesh setup of  $6.32 \times 10^7$  grids. This generally requires 156 h of central processing unit (CPU) time to complete a converged steady-state solution on an Intel Core®i7 X900-3.5 GHz (128 GB RAM) high-performance workstation.

The accuracy of the air flow field from the CFD simulations must be validated before obtaining correct estimates of the outdoor

thermal comfort. To evaluate the accuracy of the CFD simulations, three CFD simulation cases are first conducted for the three days (July 9, 13 and 17) and compared with the corresponding data from the on-site measurements, as shown in Fig. 5(a). In practice, we adopted the average reference on-site measured speeds of 3.72, 2.93 and 4.84 m/s (on July 9, 13 and 17) separately to calculate the neutral ABL velocity, turbulent kinetic energy and turbulence dissipation rate profiles, as the incoming wind flow conditions at the inlet of the computational domain [72,73]. Fig. 5(a) shows a comparison of the CFD predictions with the wind speed measurements (average values in the recorded period). As can be observed, the numerical and experimental results have a fair agreement in general for the three days. The three linear regression lines of the magnitude of the air velocity between the CFD predictions and on-site measurements all show similar tendencies and have a slope close to 1 (with an  $R^2$  greater than 0.96). The performance of the numerical simulations is thus validated since the average of the reference air velocity measured on July 17 at Point R in Fig. B.1 of the Appendix is 4.84 m/s, which is close to the most probable wind speed of 4.85 m/s obtained from a local meteorological station shown in the wind rose chart for Xinsheng Park in July 2014 (presented later in Fig. 3(a)). Furthermore, the sunshine rate and air temperature on July 17 are very close to the average of the July values collected by a local meteorological station (courtesy of the Central Weather Bureau). Therefore, only the on-site measurements on July 17, 2014, which are assumed to reflect the microclimate of Xinsheng Park in the summer (July) of 2014, will be presented here and compared with the numerical simulations due to limitations in space. The reason for choosing this month is primarily because parks would have a stronger cooling effect in the summer than winter, and the cooling effect is also much stronger at noon compared to the evening, according to the temperature measurement results in Chang et al. [54].

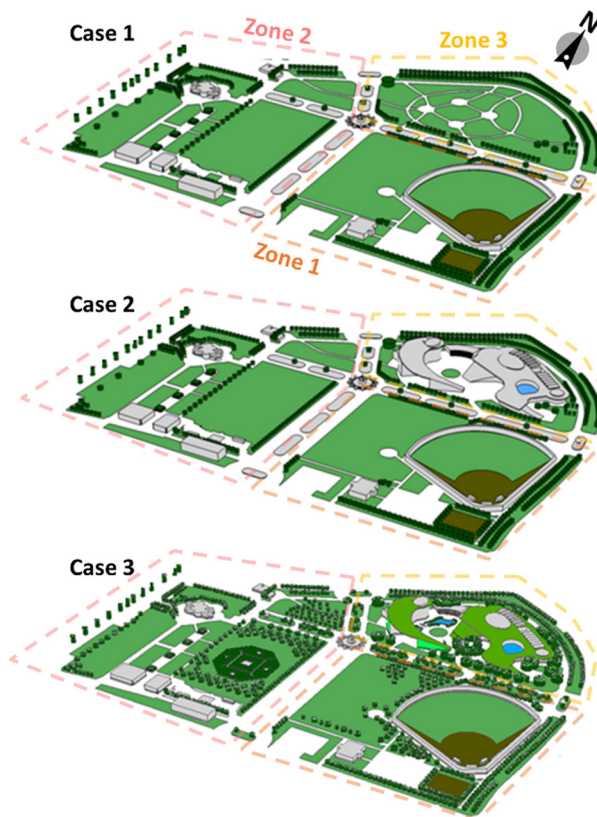
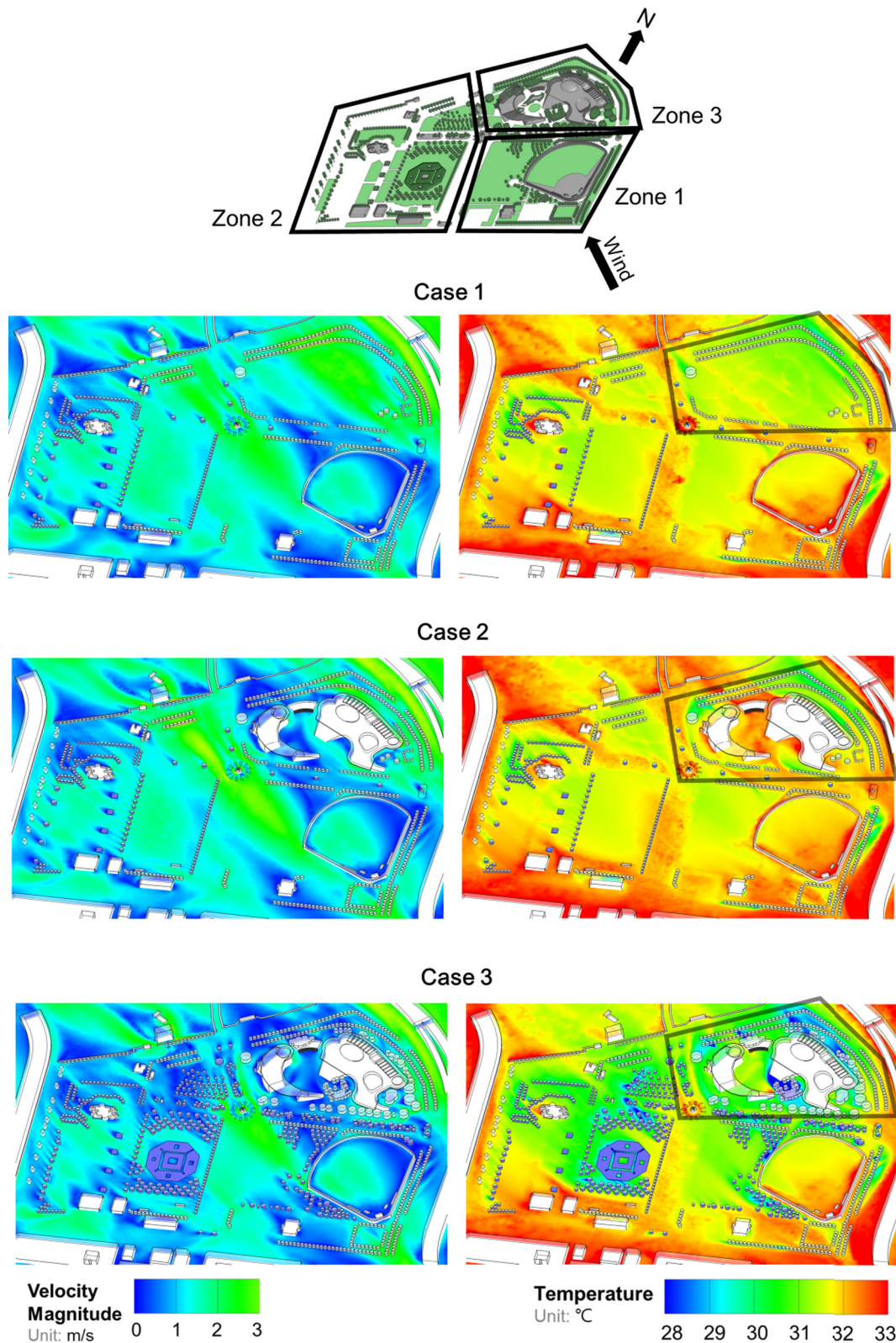


Fig. 7. Three cases: various types of greening and associated coverage ratios.

Model Area, %	Case 1	Case 2	Case 3
Building coverage	16.9	30.2	16.8
Tree coverage	17.5	14.9	21.9
Grass coverage	48.9	39.6	35.8
Green roof coverage	-	-	13.9
Hard Paving	16.7	15.3	11.6
<b>Total</b>	100	100	100

**Fig. 5(b)** shows a comparison of the CFD predictions with measurements of the magnitude of the air velocity, wind direction and temperature at different monitoring locations on July 17. Each data point denotes the average value in the recorded period. The standard deviations of the magnitude of the air velocity, wind direction

and air temperature range between 0.06–0.72 m/s, 1.5–15.6° and 0.1–0.9 °C, respectively. The results indicate the airflow that transverses the park over the grass or promenades at a speed that varies from 2.07 to 2.87 m/s, while the reference air velocity at Point R is 4.84 m/s, which is consistent with the incoming wind speed from



**Fig. 8.** Predicted magnitude of air velocity and temperature contours at height of 1.75 m as representative of conditions with average values in the hottest month.

the southeast of Xinsheng Park in July 2014. Overall, the predicted velocities at the locations in the windward region agree reasonably well with the measured data with discrepancies less than 10%. In contrast, due to the blockage from the buildings and trees, the velocities at the points on the leeward region are generally less than 1.7 m/s, with a difference up to approximately 20% between the predictions and measurements. It was noted that the discrepancies between the simulated and measured velocities are 18.3–21.4% at Positions F, M and L due to the difficulties of modeling real

tree crown characteristics in the CFD calculations. In Fig. 5(b), the predictions moderately agree in general with the measured data of the wind direction (with differences less than 10%). However, the computed wind directions at the monitored points of E, F and M deviate from those of the measured data by 11.5–16.3%, owing to relatively large variations that are a result of the low wind speeds near the trees. Fig. 5(b) also shows a fair agreement between the CFD predictions and measured temperature distribution with deviations under 10%. Besides, the outdoor air tempera-

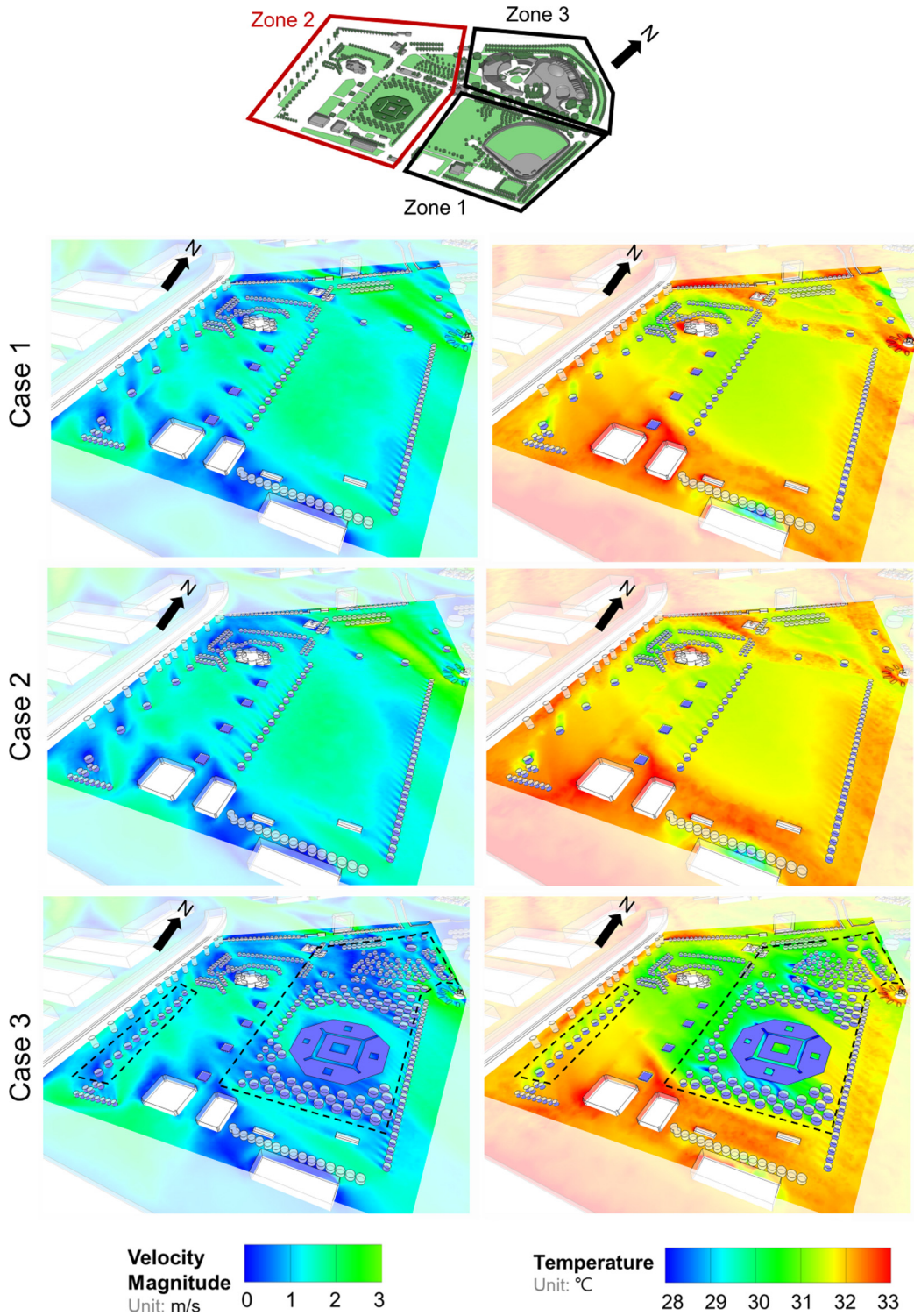


**Fig. 9.** Predicted magnitude of air velocity and temperature contours at height of 1.75 m in Zone 2.

tures vary between 27.1 °C and 32.2 °C depending on whether there is solar radiation heating on the structures and/or tree-shaded surfaces, whereas the mean radiation temperature is 30.4 °C.

**Fig. 6** shows a comparison of the CFD predictions with the surface temperature images visualized by using an infrared camera at different monitoring locations in Xinsheng Park. The infrared images (in the middle) are taken from 11:30 to 12:30 h on July 17, 2014, with the real scene photos and CFD predictions shown in the left and right columns, respectively. The temperature range is set at the same level of 25–60 °C for comparison purposes. As depicted in **Fig. 6(a)**, the surface temperatures for the roof of the Pavilion of Dreams and the top region of the tree canopy could be up to 50 °C and 35 °C, respectively, which are attributed to the direct exposure to sunlight. In **Fig. 6(b)**, the shadow effect of the tree crowns notably affects the resultant surface temperatures. The vegetative tree canopy could shade the grass by intercepting the solar radiation as well as cooling the air by evapotranspiration, and thereby result in relatively lower surface temperatures (~27 °C marked by dark blue color) for the grass areas. In contrast, **Fig. 6(c)** shows that the surface temperatures of the grass without any shading could be up to 35 °C (marked with a light blue color). In **Fig. 6(d)**, it can be observed that the outer surfaces of the concrete and asphalt reach temperatures of 37–45 °C, whereas the surface temperatures for the areas shielded by planted native trees and shrubs could be reduced to around 35 °C. In general, the comparison of the CFD predictions with the thermal images of the surface temperature showed consistency, thus indicating that the CFD simulation model in this study can predict the thermo-flow behavior over the park with reasonable accuracy. However, some noted differences were found in the spots around drop-shadow areas with the largest error up to 17% due to insufficiency of the CFD model to perfectly realistically simulate the geometric shapes of trees.

In this research, a real renewal process of the realistic urban public park was simulated. The numerical study was carried out with the detailed geometries of tree, grass, green roof, hard paving and buildings to examine the effects of vegetation on the improvement of urban microclimate. The CFD simulations were conducted to examine the cooling potential of different greening modifications on urban microclimates by considering the original form of Xinsheng Park (before renewal) as Case 1, the addition of the three pavilions to the park (after renewal) as Case 2, and realization of the supplementary green areas as Case 3 (the current form). **Fig. 7** shows the three cases with various types of greening and the related coverage ratios with Case 1 as the baseline condition. In this case, the trees/shrubs and grass envelope 17.5% and 48.9% of the total hard paving area, respectively, thus corresponding to

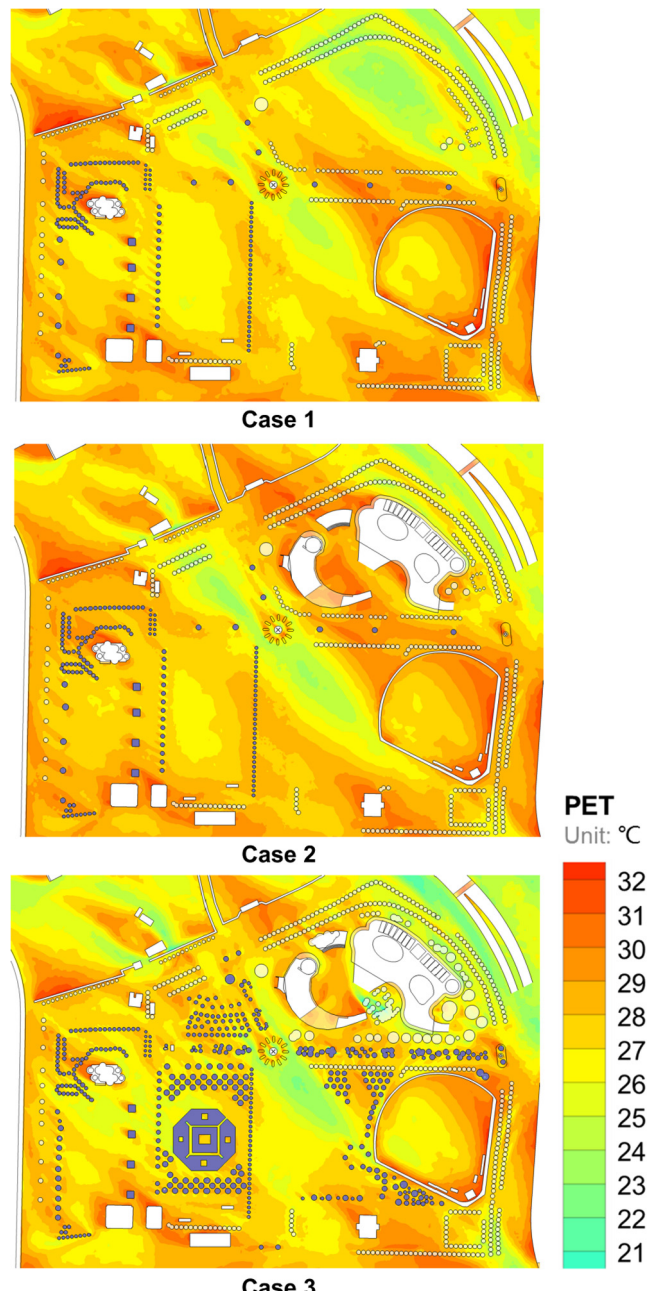


**Fig. 10.** Predicted PET contours at height of 1.75 m.

**Table 2**

Average temperature differences for different greening modifications.

Coverage area ratio (%)		Building coverage (%)	Average temperature difference $\Delta T$ (°C)
Tree	Grass		
<i>(a) Addition of three pavilions (Difference between Cases 1 and 2)</i>			
Zone 1	+0.0	+0.0	+0.1
Zone 2	+0.0	+0.0	-0.2
Zone 3	-2.6	-11.2	+1.1
Coverage area ratio (%)		Building coverage (%)	Average temperature difference $\Delta T$ (°C)
Tree	Grass & roof		
<i>(b) Addition of trees and grass roofs (Difference between Cases 2 and 3)</i>			
Zone 1	+0.3	-3.6	-0.6
Zone 2	+2.4	-8.1	-1.1
Zone 3	+4.3	+21.8	-2.4

Note: GCR = green coverage ratio; Zone 1 includes a baseball field and large open space; Zone 2 enlarges the green areas by arranging trees to develop a labyrinth and a cluster of bushes after denser greenery in Case 3. Zone 3 corresponds to a large unused flat area without built structures in Case 1, blocked by the three pavilions in Case 2 and with planting trees and grass around the pavilions in Case 3.

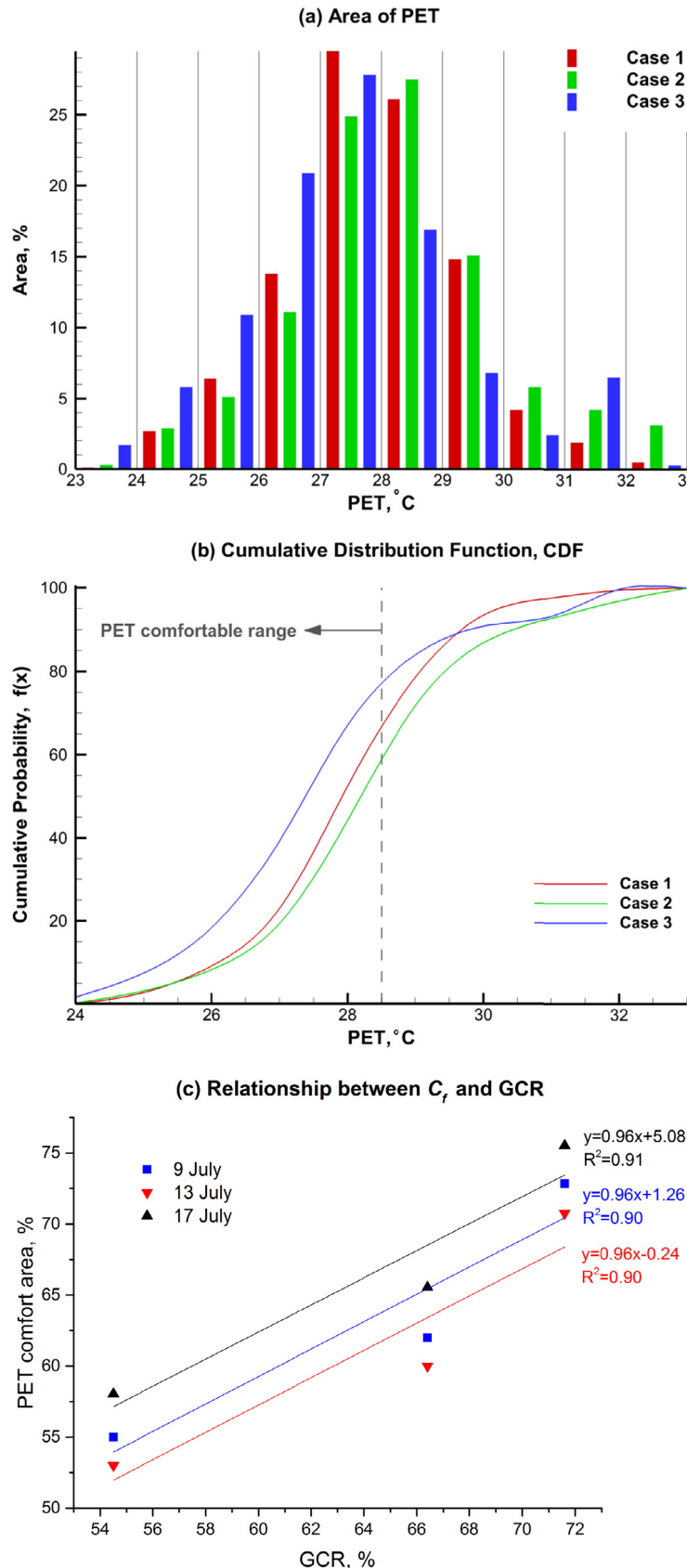


**Fig. 11.** (a) Area percentage distribution; (b) corresponding cumulative probability versus PET at height of 1.75 m over Xinsheng Park and (c) relationship between  $C_f$  and GCR.

a GCR of 66.4%. In Case 2, the three pavilions were constructed in the park with only limited existing vegetative areas removed to attain a GCR of 54.5%, whereas the overall GCR of the park increased to 71.6% after more trees were planted and the grass on the roof of the three pavilions were cultivated in Case 3.

**Fig. 8** shows the predicted magnitude of the air velocity and temperature contours at a height of 1.75 m at the pedestrian level. The simulated results were used to gain a better understanding of the effects of different greening modifications on the thermal and flow fields in park renewal processes. The color bar charts of the magnitude of the air velocity and temperature contours were retained within the same ranges for ease of comparison. In considering that the airflow is blowing over Xinsheng Park from the south east at a speed of 4.85 m/s, the predicted velocity distribution at the pedestrian level before the park renewal revealed that the fresh airflow that enters the park is partially blocked by a baseball field with a wind speed that ranges from 0.4 to 1.7 m/s on both sides of the audience area. High air velocities of up to 3 m/s (in green color) can be observed in the center and upper right region of the park owing to the relatively lower flow resistance of flat hard paving surfaces. In Case 2, high air velocities only appeared in the middle of the park with a significant decrease in the air velocity around the three pavilions. In Case 3, an increase in the flow resistance resulted from the supplementary plants which caused a drop of the airflow speed that ranged approximately 0.3–1.5 m/s in the green areas (i.e. a labyrinth and a cluster of bushes). In consideration of the outdoor thermal environments, it was observed that the presence of the three pavilions in Case 2 produces elevated temperatures (up to around 32–33 °C), as compared to the temperatures of 30.6–31.8 °C for the case where there are no built structures in Case 1. Furthermore, the CFD predictions obviously revealed the reduction of the temperature to 28.8–31.3 °C after adding the aforementioned green areas of trees and other plants to cool the environment in Case 3, thus demonstrating that vegetation a simple and useful way to reduce UHIs.

Numerical calculations were further conducted to achieve a better understanding of the outdoor thermo-flow environments for the three zones in Xinsheng Park. **Fig. B.3** in the Appendix illustrates the predicted velocity magnitude and temperature contours at a height of 1.75 m in Zone 1 which has a baseball field and large open space. The predictions in Cases 1 and 2 revealed very similar velocity distributions of around 0.4–2.5 m/s with the wind speed is reduced to 0.2–1.7 m/s in the wake region behind the baseball field. It was also observed that higher air velocities vary from 1.7 to 2.8 m/s in the large open space. Without any shading, the temperatures could increase up to 33 °C and 32 °C nearby the concrete stands of the audience area and in the large open space, respectively. Then again, for Case 3 after the park renewal, the airflow velocities were reduced to 0.3–1.5 m/s in the large open space with a reduction in the air temperatures to 29.3–30.8 °C which are attributed to the effects of shade and evapotranspiration from the additional green areas of trees around the baseball field on the windward side.

In **Fig. 9**, which shows the simulated results of Zone 2, comparable velocity and temperature fields for Cases 1 and 2 are found with corresponding ranges of 0.5–3 m/s and 31.2–32.8 °C, respectively. The higher temperature regions appear to be adjacent to the architectural constructions. However, the air temperatures are reduced to 29.1–31.4 °C after increasing the green areas by arranging trees to develop a labyrinth and a cluster of bushes in Case 3. The cooling effects that resulted from the denser greenery obviously improve the outdoor thermal environment over the open urban space. In **Fig. B.4** in the Appendix, which shows the CFD predictions in Zone 3, the wind speed and temperature range between 1–3 m/s and 30–32 °C over a large unused flat area without built structures in Case 1. In terms of Case 2, the predictions reveal a

substantial reduction of the wind speed to 0.5–2.3 m/s because of the blocking by the three pavilions. On the other hand, the outdoor temperatures increase up to 33 °C as a consequence of the direct exposure to solar radiation and lack of greenery in that area. Although the wind speed distributions for Cases 2 and 3 are similar, the computed results of Case 3 reveal a notable temperature difference between the states with and without planting trees and grass around the pavilions. The ambient temperatures are reduced to 29.1–31.4 °C due to the additional green areas, as compared to those in Case 2.

**Table 2** demonstrates the average temperature differences for different greening modifications. As compared to the baseline (Case 1), that is, the original layout of Xinsheng Park (before park renewal), the simulation results reveal that the mean value over the temperature distribution is increased by 1.1 °C after the park renewal (Case 2), and when the three pavilions were constructed, the building coverage increased by 13.8% in Zone 3. To realize the supplementary green areas in Case 3, the average temperatures are relatively reduced by 0.6 °C and 1.1 °C in Zones 1 and 2 as a result of increased tree coverage ratios of 0.3 and 2.4%, while the grass coverage ratios are lowered by 3.6 and 8.1%, respectively. It shows that the slightly increased tree coverage ratio could still reduce the average temperature to achieve a cooler locality. Though the LAD of trees is less than that of lawn, the trees can block shortwave radiation of the sun and absorb long-wave radiation of the ground, which would greatly reduce the air temperature and improve thermal comfort. Accordingly, the cooling effect from tree shade tends to be more effective than that from the evapotranspiration of grass due to the sun-blocking effect of trees. Moreover, the augmented tree/grass coverage ratios of 4.3/21.8% could reduce the average temperatures in Zone 3 by 2.42 °C to achieve a cooler locality. **Table A.3** shows a comparison of the reduction in the air temperature due to urban greening in different climates. The climate types are categorized in accordance with the Köppen climate classification [82]. As can be observed, many other researchers have also presented similar results for other subtropical areas. For instance, Saito et al. [50] reported a measured maximum temperature difference of 3 °C between the inside and outside of the green area in the summer for Kumamoto City, Japan. Katayama et al. [51] found that an increase in the GCR from 0 to 100% resulted in a reduced air temperature reduction of 2.7 °C during the summer period in Fukuoka City, Japan. Srivani and Hokao [37] proposed that the average maximum temperature decreases and increases by 2.27 °C during the peak hours in the summer (at 15:00) if the quantity of trees is increased by 20% in Japan. The measured results from Hamada and Ohta [9] revealed that the maximum difference in the air temperature between the urban and green areas is 1.9 °C in July 2007. The temperature was found to be closely related to the forest-cover ratio within a radius of 200 m from each measured site. Likewise, in other different climate zones, Oliveira et al. [13] even observed a highest temperature difference of 6.9 °C between the shaded and open sites near a garden during the hottest month of the year in Lisbon, Portugal. Although there is no clear correlation between air temperature reduction and climate type, the different research work has shown temperature reductions to a certain degree. The above studies positively support the cooling consequences of greening areas for improving urban environments and mitigation of UHI effects. However, compared to the research in the literature, we have included, in addition, the urban renewal process in a subtropical zone of Taiwan and incorporated green spaces into the urban planning.

In view of thermal comfort, the PET index has been designed for outdoor use because it considers the effects of the mean radiant temperature, clothing, and metabolic rates of the space users [25]. The details of the PET calculation includes the following

steps: (1) Calculating the thermal conditions of the body with MEMI for a given combination of meteorological parameters; (2) Inserting the calculated values for mean skin temperature and core temperature into the MEMI model and solving the energy balance equation system for air temperature, which to PET. In this study, as a thermal indicator derived from the energy balance of the human body to calculate the PET, the values of activity, the metabolic rate and clothing insulation were prescribed as 80 W, 1.2 met and 0.9 clo, respectively. Besides, the measured results were employed to determine the relative humidity (62%) and the mean radiation temperature (36 °C), whereas the values of the air temperature and velocity in the areas of interest were acquired from CFD computations. The PET was estimated by applying the RayMan model, which has been used in urban built-up areas with complex shading patterns for accurately predicting thermal comfort environments [24]. It should be noted that the measured values of relative humidity and mean radiation temperature (62% and 36 °C) approximate the average relative humidity and radiation temperature from 10 years of climatological data (62% and 36 °C), which were recorded at a local meteorological station for the period of 2004–2014 in the summer. Fig. 10 illustrates the predicted PET contours at a height of 1.75 m for the three cases. According to ASHRAE Standard 55, acceptable thermal conditions must be found to be satisfactory by a minimum of 90% of the occupants in a space when a high standard is used [83]. Based on a study by Lin [24] on classification of thermal perception, the results showed the thermally comfortable range of 21.3–28.5 °C in the PET in Taipei with a state of discomfort defined as the thermal condition outside this temperature range, i.e., PET > 28.5 °C or PET < 21.3 °C. The scenario in Case 1 primarily considers the grassy areas without dense canopy covers, and thus the predictions showed a PET range of 24–28.5 °C in the open spaces of the park. Therefore, visitors may feel uncomfortable in the areas around architectural constructions (with a PET range of 29–32 °C), especially around the baseball field. In Case 2, the areas around the buildings have a PET that is higher than 28.5 °C, and the areas near the three pavilions have a PET between 30 and 32 °C, which is uncomfortable, thus suggesting that the cooling effect from the greening layout is not sufficient enough to provide thermal comfort for the entire Xinsheng Park. From the predicted PET contours in Case 3, the use of trees and grass tends to provide a shading effect to protect land or building surfaces from solar heat, and thereby led to a reduction in the PET to 21–23 °C (marked in light blue). Therefore, users will experience thermal comfort around vegetation and grass areas with improved outdoor microclimates in the park. Due to the variations of the thermal index, the PET is mostly affected by temperature rather than airflow speed. The simulation results suggest that large canopy trees that are properly spaced apart can be designed and aligned with respect to a solar diagram so as to provide good shading that would improve the thermal comfort of visitors in outdoor public spaces.

Fig. 11 illustrates (a) the area percentage distribution versus PET and (b) the corresponding cumulative distribution function, which shows the PET probability at a height of 1.75 m over Xinsheng Park. For the three greening scenarios in the renewal development of the park, the area percentages show approximately normal distributions with respect to the PET. In considering a PET range between 21.3 and 28.5 °C as thermally comfortable, the cumulative distribution functions indicate that the estimated area percentages are 65.6%, 58.0%, and 75.6% for the thermally comfortable areas (termed as percentage of areas that are comfortable,  $C_f$ ) for Cases 1, 2 and 3, respectively. A higher  $C_f$  value can be noted for Case 3, thus suggesting a greater probability of a thermally comfortable state that is attributed to an increase in the GCR. Fig. 11(c) shows the relationship between the  $C_f$  and GCR

(in%) for July 17, as representative of conditions with average values in the hottest month, is shown in Fig. 11(c). A linear regression analysis is used to determine the correlation between  $C_f$  and GCR, which yields  $C_f = 0.96 \times \text{GCR} + 5.08$  with the sum of  $R^2$  of 0.91, for GCR ranged from 54.5 to 71.6% in this study. Essentially, the thermally comfortable areas in the park measured by PET monotonically increase with GCR. This shows a significant alleviation of the UHI effect with increased GCR. Gromke et al. [63] also observed that the resultant temperature field inside a street canyon resembled a linear superposition of the cooling from spatial distribution and intensity of all vegetative measures in the city center of Arnhem, the Netherlands. Notably, the linear regression analyses performed on the other two days (July 9 and 13) essentially yield nearly the same correlation between  $C_f$  and GCR as in Fig. 11(c) (July 17). As shown, the same slope can fit the three day data equally well, with the sum of  $R^2$  of 0.90 and above. The slight difference in the intercept values may be caused by the different air temperatures and wind velocities (Table 1) in three days. More data will be collected from other public parks in Taiwan to further validate the linear relationship in future studies.

#### 4. Conclusions

The objective of this study is to investigate the effects of vegetation on mitigation of UHI effects after the renewal of the public park in a subtropical climate. Numerical simulations and field measurements are performed to examine the thermo-flow behaviors in an urban park, which will provide architects and planners with a better understanding of the park design by probing the impacts of three newly added pavilions and supplementary green areas on the urban microclimate. This study points out that vegetation can mitigate urban heat islands directly with shading by tree canopy, and indirectly through evaporation cooling. Furthermore, urban parks support city ventilation, which is an imperative aspect for the mitigation of the urban heat island effect. The park breeze is important for city breathability, which is based on temperature differences as a driving force. It has proved that additional green areas are cool patches in the public park renewal process. Especially, the climate inside the urban parks tends to be cooler than that in their urban surroundings. This phenomenon is often referred to as the "Park Cool Island" effect. We have also elucidated the PET distributions over the entire park for three cases. The primary results are summarized as follows.

- (1) From the predicted magnitude of the air velocity and temperature contours, it can be seen that trees and vegetation are effective for shading buildings from solar radiation, and accordingly reduce the surface temperature of the different environments. A comparison of the simulated results of the different greening modifications indicates an average temperature increase of 1.1 °C from the three pavilions constructed with an increased building coverage of 13.8% in Zone 3. In addition, the average temperature is reduced by 2.42 °C which contributes to a cooler locality due to the augmented tree/grass coverage ratios of 4.3/21.8% in Zone 3.
- (2) The GCR is a key factor that affects the cooling outcome, and in this case, for the park. The thermal comfortable area can be nonlinearly related to the green coverage ratio in nature, nevertheless, for expedient applications, a linear regression between the GCR and PET reveals a greater probability of thermal comfort with an increase in the GCR. The findings therefore provide a useful measure with the implementation of greening modifications in public parks to enhance cooling for the mitigation of the UHI effect in a subtropical region.

The limitation of this study will be addressed in future work:

- (1) Steady computations were performed to simulate the scenarios of average conditions during the hottest month of the year. It may disregard the temporal fluctuations in wind velocity, direction and diurnal temperature amplitude.
- (2) Detailed distinctions of land-cover such as different building materials, water bodies, soil moisture content and artificial heat release were not considered in this study. Those issues

can be included in future investigations to improve the prediction accuracy for actual urban environments.

### Acknowledgment

Some of the results in this paper were obtained with the support of the National Science Council, Taiwan, ROC (Contract No. MOST 104-2221-E-027-118).

### Appendix A

See Tables A.1–A.3.

**Table A.1**  
Micrometeorological variables and sensors used for measurement.

Sensor	Variable	Range	Accuracy
WindMaster 3D Sonic Anemometer, Gill Instruments Limited	Air wind velocity	0–45 m/s	<1.5 RMS
	Wind direction	0–359°	2°
Thermal flow probe, Testo 0635 1543	Air temperature	–20 to 70 °C	±0.5 °C
Globe probe, Testo 0602 0743	Globe temperature	0 to +120 °C	Class 1
Avio/NEC, H2640	Thermal imager	–40 to 500 °C	±2 °C or ±2%

**Table A.2**  
Spectral optical and thermos-physical material properties [77].

Property	Fluid	Building	Ground	Plants
Materials	Air	Concrete	Asphalt	Porous materials
Density (kg/m <sup>3</sup> )	1.225	2400	2360	700
Specific heat (J/kg K)	1006.43	750	920	2310
Thermal conductivity (W/m K)	0.0242	1.7	0.75	0.173
Viscosity (kg/m S)	$1.7894 \times 10^{-5}$	–	–	–
Absorption coefficient (1/m)	0.19	0.9	0.9	0.46
Scattering coefficient (1/m)	0	0	–10	0
Refractive index	1	1.7	1.92	2.77
Emissivity, ε	0.9	0.7	0.95	0.46

**Table A.3**  
Comparison of reductions in air temperature from urban greening in different climates.

Climate type: Köppen climate classification	City/Country	Difference in air temperature	Reference
Humid subtropical climate	Taipei, Taiwan	The augmented tree/grass coverage ratios of 4.3/21.8% could reduce the average temperature by 2.42 °C	Current study
Humid subtropical climate	Kumamoto, Japan	The cooling effect of a small green area with the size of 60 m × 40 m caused the maximum temperature difference of 3 °C inside and outside the green area in summer	[50]
Humid subtropical climate	Fukuoka, Japan	The ratio of natural covering from 0% to 100% resulted in a decrease of air temperature by 2.7 °C during the summer	[51]
Humid subtropical climate	Fukuoka, Japan	The average maximum temperature would decrease 2.27 °C in the peak of the summer (at 15:00)	[37]
Humid subtropical climate	Nagoya, Japan	The maximum temperature difference between the urban and green areas reached approximately 1.9 °C in the summer	[9]
Mediterranean climate	Athens, Greece	The total attenuation effect in reducing the air temperatures inside the streets may reach as much as 5 °C at noon time with a daily average cooling of 3 °C	[49]
Desert climate	Dubai	The inclusion of the green plants can possibly eliminate high temperature in urban areas in Dubai, ranging from 2 °C to 6 °C	[10]
Mediterranean climate	Lisbon, Portugal	The greatest temperature difference was 6.9 °C, which occurred between a shaded site in the garden and a sunshine site during the hottest month of the year	[13]
Tropical rainforest climate	Singapore	The average temperature difference of 1.3 °C was observed at locations around the parks	[84]

## Appendix B

See Figs. B.1–B.4.

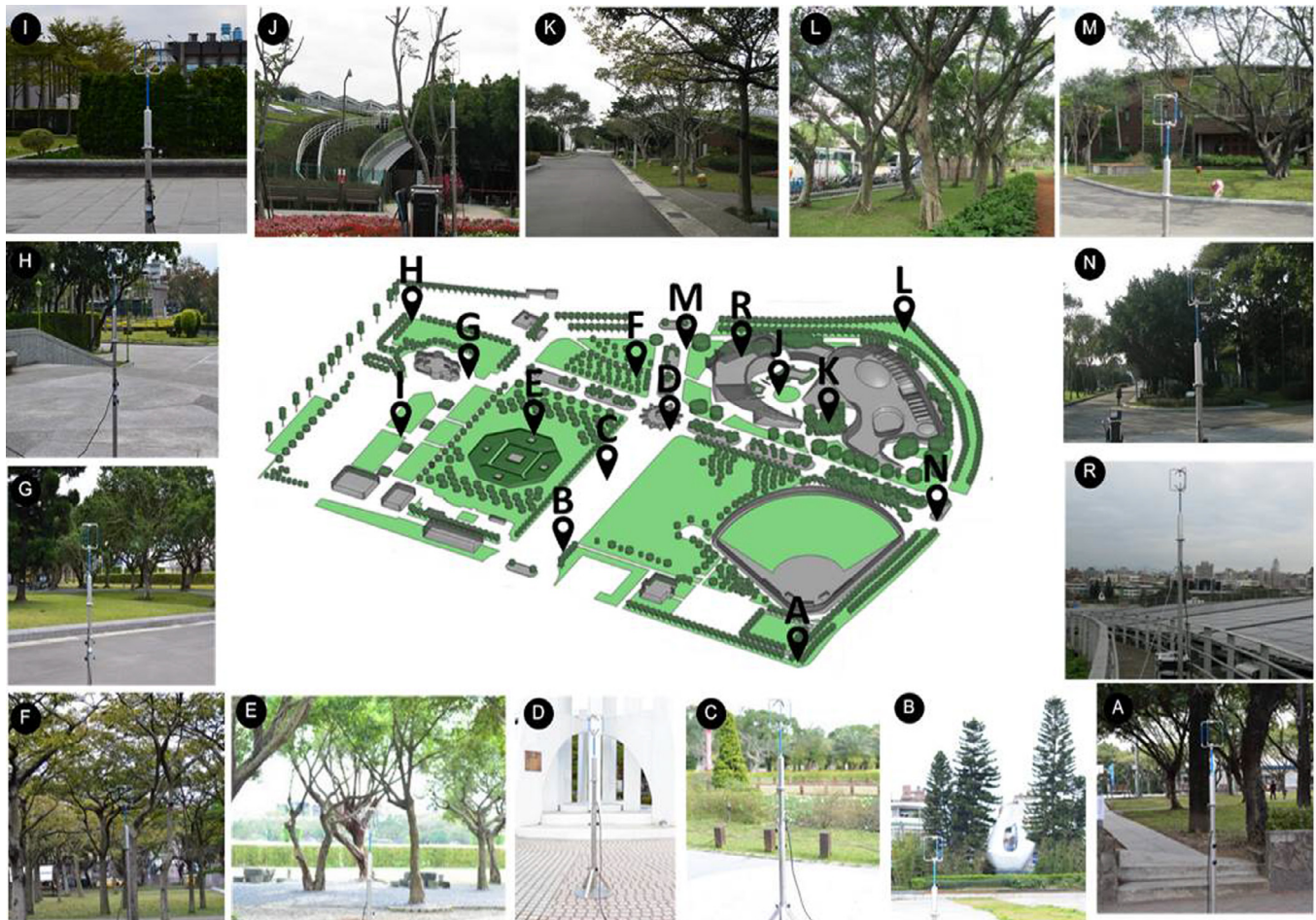


**Fig. B.1.** Photographs and locations of the 15 monitoring points in Xinsheng Park.

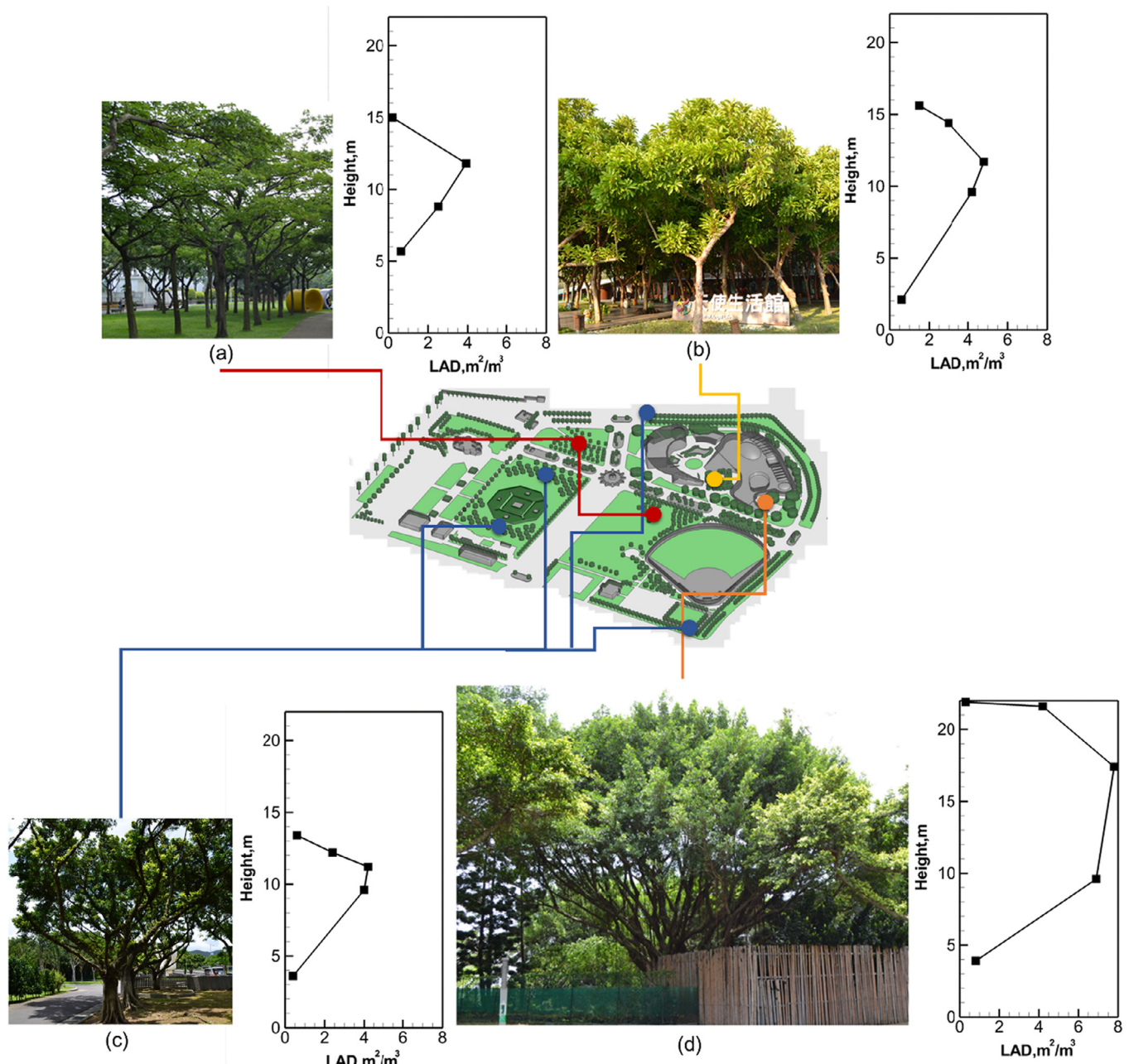


**Fig. B.2.** Locations and leaf area densities of four types of trees in Xinsheng Park: (a) *Sterculia foetida*, (b) *Dillenia indica*, (c) *Ficus microcarpa* and (d) *Ficus benjamina*. Numerical modeling of Xinsheng Park in center considers trees as one-dimensional column with given normalized leaf area density profile with height.

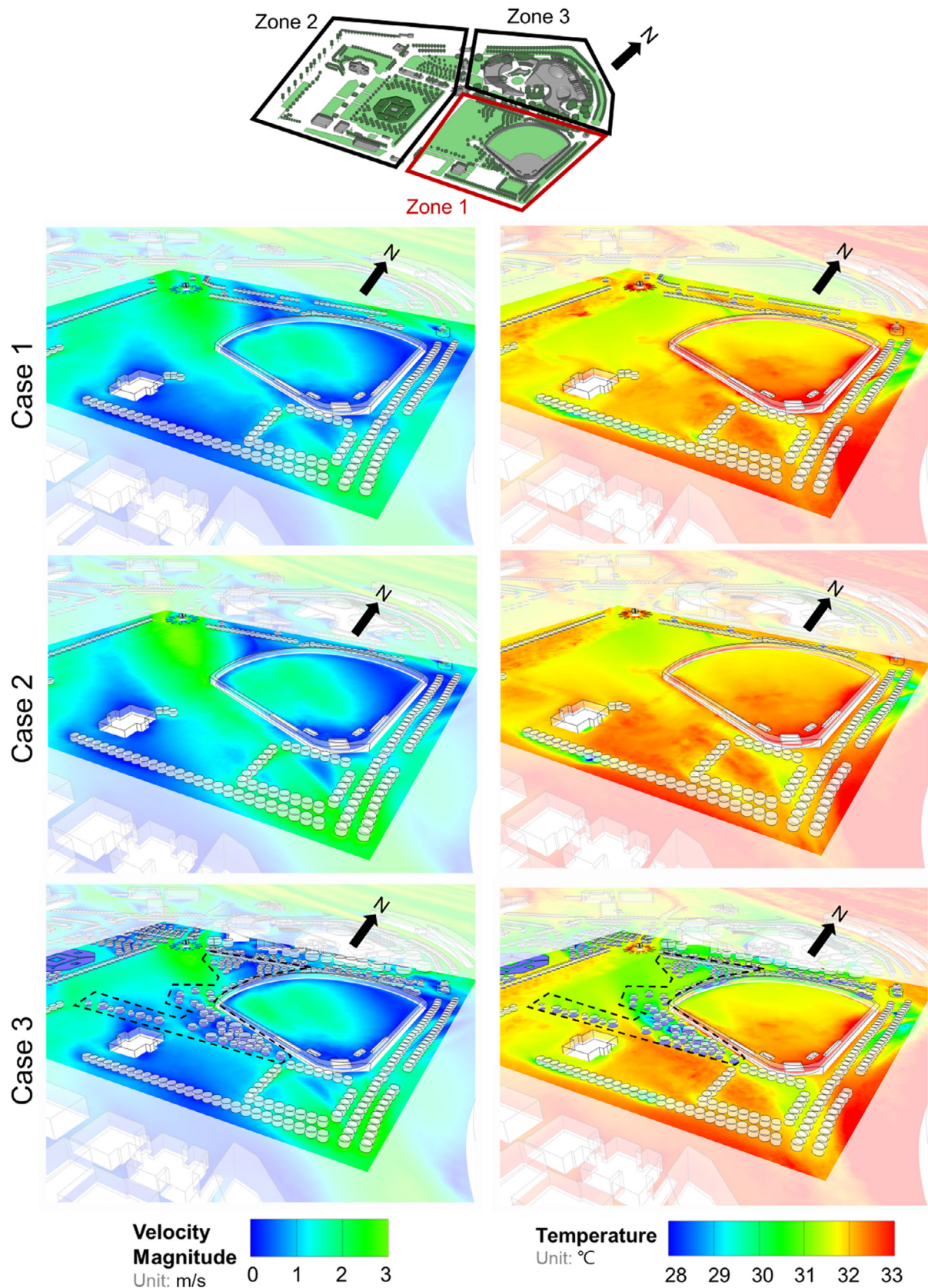


Fig. B.3. Predicted magnitude of air velocity and temperature contours at height of 1.75 m in Zone 1.

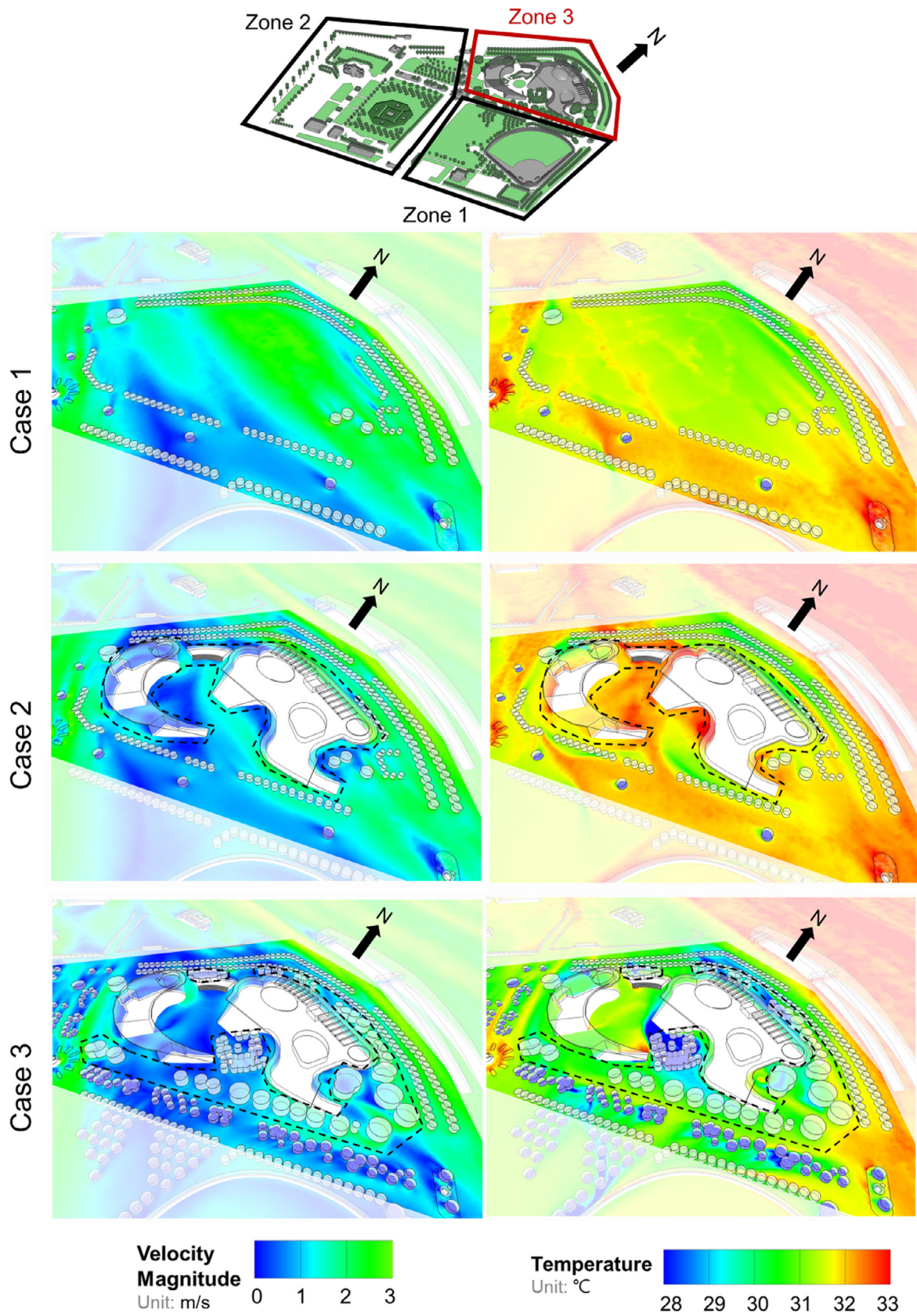


Fig. B.4. Predicted magnitude of air velocity and temperature contours at height of 1.75 m in Zone 3.

## References

- [1] Yang L, Yan H, Lam JC. Thermal comfort and building energy consumption implications – a review. *Appl Energy* 2014;115:164–73.
- [2] Ng E, Chen L, Wang Y, Yuan C. A study on the cooling effects of greening in a high-density city: an experience from Hong Kong. *Build Environ* 2012;47:256–71.
- [3] Yang A-S, Wen C-Y, Juan Y-H, Su Y-M, Wu J-H. Using the central ventilation shaft design within public buildings for natural aeration enhancement. *Appl Therm Eng* 2014;70:219–30.
- [4] Kim J, Hong T, Jeong J, Koo C, Jeong K. An optimization model for selecting the optimal green systems by considering the thermal comfort and energy consumption. *Appl Energy* 2016;169:682–95.
- [5] Jim CY. Air-conditioning energy consumption due to green roofs with different building thermal insulation. *Appl Energy* 2014;128:49–59.
- [6] Berardi U, GhaffarianHoseini A, GhaffarianHoseini A. State-of-the-art analysis of the environmental benefits of green roofs. *Appl Energy* 2014;115:411–28.
- [7] Ouldboukhite S-E, Belarbi R, Sailor DJ. Experimental and numerical investigation of urban street canyons to evaluate the impact of green roof inside and outside buildings. *Appl Energy* 2014;114:273–82.
- [8] Zoula I, Santamouris M, Dimoudi A. Monitoring the effect of urban green areas on the heat island in Athens. *Environ Monit Assess* 2008;156:275–92.
- [9] Hamada S, Ohta T. Seasonal variations in the cooling effect of urban green areas on surrounding urban areas. *Urb Forest Urb Greening* 2010;9:15–24.
- [10] Taleb H, Taleb D. Enhancing the thermal comfort on urban level in a desert area: case study of Dubai, United Arab Emirates. *Urb Forest Urb Greening* 2014;13:253–60.
- [11] Dimoudi A, Nikolopoulou M. Vegetation in the urban environment: microclimatic analysis and benefits. *Energy Build* 2003;35:69–76.
- [12] Shashua-Bar L, Hoffman ME. Vegetation as a climatic component in the design of an urban street: an empirical model for predicting the cooling effect of urban green areas with trees. *Energy Build* 2000;31:221–35.
- [13] Oliveira S, Andrade H, Vaz T. The cooling effect of green spaces as a contribution to the mitigation of urban heat: a case study in Lisbon. *Build Environ* 2011;46:2186–94.
- [14] Wang Z-H, Zhao X, Yang J, Song J. Cooling and energy saving potentials of shade trees and urban lawns in a desert city. *Appl Energy* 2016;161:437–44.
- [15] Rosenfeld AH, Akbari H, Bretz S, Fishman BL, Kurn DM, Sailor D, et al. Mitigation of urban heat islands: materials, utility programs, updates. *Energy Build* 1995;22:255–65.
- [16] Jaffal I, Ouldboukhite S-E, Belarbi R. A comprehensive study of the impact of green roofs on building energy performance. *Renew Energy* 2012;43:157–64.
- [17] Shahzad S, Brennan J, Theodosopoulos D, Hughes B, Calautit JK. Energy and comfort in contemporary open plan and traditional personal offices. *Appl Energy* 2017;185:1542–55.
- [18] Ascione F, Bianco N, de' Rossi F, Turni G, Vanoli GP. Green roofs in European climates. Are effective solutions for the energy savings in air-conditioning? *Appl Energy* 2013;104:845–59.
- [19] Jim CY. Thermal performance of climber greenwalls: effects of solar irradiance and orientation. *Appl Energy* 2015;154:631–43.
- [20] Eliasson I. The use of climate knowledge in urban planning. *Landscape Urb Plann* 2000;48:31–44.
- [21] Liu Y, Harris DJ. Effects of shelterbelt trees on reducing heating-energy consumption of office buildings in Scotland. *Appl Energy* 2008;85:115–27.
- [22] Wang Y, Bakker F, de Groot R, Wörtche H. Effect of ecosystem services provided by urban green infrastructure on indoor environment: a literature review. *Build Environ* 2014;77:88–100.
- [23] Simmons MT, Gardiner B, Windhager S, Tinsley J. Green roofs are not created equal: the hydrologic and thermal performance of six different extensive green roofs and reflective and non-reflective roofs in a sub-tropical climate. *Urb Ecosyst* 2008;11:339–48.
- [24] Lin T-P. Thermal perception, adaptation and attendance in a public square in hot and humid regions. *Build Environ* 2009;44:2017–26.
- [25] Gómez F, Cueva AP, Valcuende M, Matzarakis A. Research on ecological design to enhance comfort in open spaces of a city (Valencia, Spain). Utility of the physiological equivalent temperature (PET). *Ecol Eng* 2013;57:27–39.
- [26] Gulyás Á, Unger J, Matzarakis A. Assessment of the microclimatic and human comfort conditions in a complex urban environment: modelling and measurements. *Build Environ* 2006;41:1713–22.
- [27] Höppe P. The physiological equivalent temperature – a universal index for the biometeorological assessment of the thermal environment. *Int J Biometeorol* 1999;43:71–5.
- [28] Höppe P. Heat balance modelling. *Experientia* 1993;49:741–6.
- [29] Tran H, Uchihama D, Ochi S, Yasuoka Y. Assessment with satellite data of the urban heat island effects in Asian mega cities. *Int J Appl Earth Obs Geoinf* 2006;8:34–48.
- [30] Wong MS, Nichol JE, To PH, Wang J. A simple method for designation of urban ventilation corridors and its application to urban heat island analysis. *Build Environ* 2010;45:1880–9.
- [31] Wei J, He J. Numerical simulation for analyzing the thermal improving effect of evaporative cooling urban surfaces on the urban built environment. *Appl Therm Eng* 2013;51:144–54.
- [32] Bowler DE, Buyung-Ali L, Knight TM, Pullin AS. Urban greening to cool towns and cities: a systematic review of the empirical evidence. *Landscape Urb Plann* 2010;97:147–55.
- [33] Chan ALS. Developing a modified typical meteorological year weather file for Hong Kong taking into account the urban heat island effect. *Build Environ* 2011;46:2434–41.
- [34] Feyisa GL, Dons K, Meilby H. Efficiency of parks in mitigating urban heat island effect: an example from Addis Ababa. *Landscape Urb Plann* 2014;123:87–95.
- [35] Park M, Hagishima A, Tanimoto J, Narita K-i. Effect of urban vegetation on outdoor thermal environment: field measurement at a scale model site. *Build Environ* 2012;56:38–46.
- [36] Bruse M, Fleer H. Simulating surface–plant–air interactions inside urban environments with a three dimensional numerical model. *Environ Model Softw* 1998;13:373–84.
- [37] Srivanit M, Hokao K. Evaluating the cooling effects of greening for improving the outdoor thermal environment at an institutional campus in the summer. *Build Environ* 2013;66:158–72.
- [38] Svensson U, Häggkvist K. A two-equation turbulence model for canopy flows. *J Wind Eng Ind Aerodyn* 1990;35:201–11.
- [39] Alexandri E, Jones P. Temperature decreases in an urban canyon due to green walls and green roofs in diverse climates. *Build Environ* 2008;43:480–93.
- [40] Taha H. Urban climates and heat islands: albedo, evapotranspiration, and anthropogenic heat. *Energy Build* 1997;25:99–103.
- [41] Fröhlich D, Matzarakis A. Modeling of changes in thermal bioclimate: examples based on urban spaces in Freiburg, Germany. *Theor Appl Climatol* 2013;111:547–58.
- [42] Vidrih B, Medved S. Multiparametric model of urban park cooling island. *Urb Forest Urb Greening* 2013;12:220–9.
- [43] Mochida A, Tabata Y, Iwata T, Yoshino H. Examining tree canopy models for CFD prediction of wind environment at pedestrian level. *J Wind Eng Ind Aerodyn* 2008;96:1667–77.
- [44] Yang F, Lau SSY, Qian F. Summertime heat island intensities in three high-rise housing quarters in inner-city Shanghai China: building layout, density and greenery. *Build Environ* 2010;45:115–34.
- [45] Amorim JH, Rodrigues V, Tavares R, Valente J, Borrego C. CFD modelling of the aerodynamic effect of trees on urban air pollution dispersion. *Sci Total Environ* 2013;461:462–541–51.
- [46] Yang AS, Juan YH, Wen CY, Su YM, Wu YC. Investigation on wind environments of surrounding open spaces around a public building. *J Mech* 2016;1–13.
- [47] Wen C-Y, Juan Y-H, Yang A-S. Enhancement of city breathability with half open spaces in ideal urban street canyons. *Build Environ* 2017;112:322–36.
- [48] Taleghani M, Tempierik M, van den Dobbelaer A, Sailor DJ. Heat mitigation strategies in winter and summer: field measurements in temperate climates. *Build Environ* 2014;81:309–19.
- [49] Shashua-Bar L, Tsioris IX, Hoffman ME. A modeling study for evaluating passive cooling scenarios in urban streets with trees. Case study: Athens, Greece. *Build Environ* 2010;45:2798–807.
- [50] Saito I, Ishihara O, Katayama T. Study of the effect of green areas on the thermal environment in an urban area. *Energy Build* 1990;15:493–8.
- [51] Katayama T, Ishii A, Hayashi T, Tsutsumi J-i. Field surveys on cooling effects of vegetation in an urban area. *J Therm Biol* 1993;18:571–6.
- [52] Zhang Z, Lv Y, Pan H. Cooling and humidifying effect of plant communities in subtropical urban parks. *Urb Forest Urb Greening* 2013;12:323–9.
- [53] Lin H-T, Lee K-P, Chen K-T, Lin L-J, Kuo H-C, Chen T-C. Experimental analyses of urban heat island effects of the four metropolitan cities in Taiwan (I) – the comparison of the heat island intensities between Taiwan and the world cities. *J Archit* 1999;31:51–73.
- [54] Chang C-R, Li M-H, Chang S-D. A preliminary study on the local cool-island intensity of Taipei city parks. *Landscape Urb Plann* 2007;80:386–95.
- [55] ISO 7726:1998. Ergonomics of the thermal environment – instruments for measuring physical quantities; 2012.
- [56] Blocken B, Janssen WD, van Hooff T. CFD simulation for pedestrian wind comfort and wind safety in urban areas: general decision framework and case study for the Eindhoven University campus. *Environ Model Softw* 2012;30:15–34.
- [57] ANSYS I. ANSYS FLUENT CFD 15.0 user's manual; 2013.
- [58] Shih T-H, Liou WW, Shabir A, Yang Z, Zhu J. A new K-epsilon eddy viscosity model for high Reynolds number turbulent flows. *Comput Fluids* 1995;24:227–38.
- [59] Karava P, Jubayer CM, Savory E. Numerical modelling of forced convective heat transfer from the inclined windward roof of an isolated low-rise building with application to photovoltaic/thermal systems. *Appl Therm Eng* 2011;31:1950–63.
- [60] Yang A-S, Su Y-M, Wen C-Y, Juan Y-H, Wang W-S, Cheng C-H. Estimation of wind power generation in dense urban area. *Appl Energy* 2016;171:213–30.
- [61] Ai ZT, Mak CM. CFD simulation of flow in a long street canyon under a perpendicular wind direction: evaluation of three computational settings. *Build Environ* 2017;114:293–306.
- [62] Robitu M, Musy M, Inard C, Croleau D. Modeling the influence of vegetation and water pond on urban microclimate. *Sol Energy* 2006;80:435–47.
- [63] Gromke C, Blocken B, Janssen W, Merema B, van Hooff T, Timmermans H. CFD analysis of transpiration cooling by vegetation: case study for specific meteorological conditions during a heat wave in Arnhem, Netherlands. *Build Environ* 2015;83:11–26.
- [64] Gromke C, Blocken B. Influence of avenue-trees on air quality at the urban neighborhood scale. Part I: Quality assurance studies and turbulent Schmidt number analysis for RANS CFD simulations. *Environ Pollut* 2015;196:214–23.

- [65] Green SR. Modelling turbulent air flow in a stand of widely-spaced trees. *PHOENICS J.* 1992;5:294–312.
- [66] Kenjeres S, ter Kuile B. Modelling and simulations of turbulent flows in urban areas with vegetation. *J Wind Eng Ind Aerodyn* 2013;123(Part A):43–55.
- [67] Incropera FP, Lavine AS, DeWitt DP. Fundamentals of heat and mass transfer. John Wiley & Sons Incorporated; 2011.
- [68] Defraeye T, Herremans E, Verboven P, Carmeliet J, Nicolai B. Convective heat and mass exchange at surfaces of horticultural products: a microscale CFD modelling approach. *Agric Meteorol* 2012;162–163:71–84.
- [69] Defraeye T, Verboven P, Derome D, Carmeliet J, Nicolai B. Stomatal transpiration and droplet evaporation on leaf surfaces by a microscale modelling approach. *Int J Heat Mass Transf* 2013;65:180–91.
- [70] Blocken B, Carmeliet J, Stathopoulos T. CFD evaluation of wind speed conditions in passages between parallel buildings—effect of wall-function roughness modifications for the atmospheric boundary layer flow. *J Wind Eng Ind Aerodyn* 2007;95:941–62.
- [71] Harrison RM, Royal Society of C. Understanding our environment: an introduction to environmental chemistry and pollution. Cambridge, UK: Royal Society of Chemistry; 1999.
- [72] Richards PJ. Computational modelling of wind flows around low rise buildings using PHOENIX. Bedfordshire, UK: Report for the ARFC Institute of Engineering Research Wrest Park, Silsoe Research Institute; 1989. p. 93–112.
- [73] Richards P, Hoxey R. Appropriate boundary conditions for computational wind engineering models using the k-turbulence model. *J Wind Eng Ind Aerodynam* 1993;46–47:145–53.
- [74] Wieringa J. Updating the Davenport roughness classification. *J Wind Eng Ind Aerodyn* 1992;41:357–68.
- [75] Chen WF, editor. Handbook of structural engineering. Boca Raton, Fla.: CRC Press; 1997.
- [76] Hargreaves DM, Wright NG. On the use of the k-model in commercial CFD software to model the neutral atmospheric boundary layer. *J Wind Eng Ind Aerodyn* 2007;95:355–69.
- [77] Fidaros DK, Baxevanou CA, Bartzanas T, Kittas C. Numerical simulation of thermal behavior of a ventilated arc greenhouse during a solar day. *Renew Energy* 2010;35:1380–6.
- [78] Palyvos JA. A survey of wind convection coefficient correlations for building envelope energy systems' modeling. *Appl Therm Eng* 2008;28:801–8.
- [79] Mirsadeghi M, Cóstola D, Blocken B, Hensen JLM. Review of external convective heat transfer coefficient models in building energy simulation programs: implementation and uncertainty. *Appl Therm Eng* 2013;56:134–51.
- [80] Jang DS, Jetli R, Acharya S. Comparison of the PISO, SIMPLER, and SIMPLEC algorithms for the treatment of the pressure–velocity coupling in Steady flow problems. *Numer Heat Transf* 1986;10:209–28.
- [81] Van Doormaal JP, Raithby GD. Enhancements of the SIMPLE method for predicting incompressible fluid flows. *Numer Heat Transf* 1984;7:147–63.
- [82] Peel MC, Finlayson BL, McMahon TA. Updated world map of the Köppen-Geiger climate classification. *Hydrol Earth Syst Sci* 2007;11:1633–44.
- [83] ASHRAE. ANSI/ASHRAE standard 55-2013: thermal environmental conditions for human occupancy. Atlanta, GA: ASHRAE; 2013.
- [84] Yu C, Hien WN. Thermal benefits of city parks. *Energy Build* 2006;38:105–20.